Titre: Title:	Hydrodynamics characterization of the maxblend impeller
Auteur: Author:	Arash Iranshahi
Date:	2006
Type:	Mémoire ou thèse / Dissertation or Thesis
Référence: Citation:	Iranshahi, A. (2006). Hydrodynamics characterization of the maxblend impeller [Master's thesis, École Polytechnique de Montréal]. PolyPublie. https://publications.polymtl.ca/7819/

UNIVERSITÉ DE MONTRÉAL

HYDRODYNAMICS CHARACTERIZATION OF THE MAXBLEND IMPELLER

ARASH IRANSHAHI

DÉPARTEMENT DE GÉNIE CHIMIQUE

ÉCOLE POLYTECHNIQUE DE MONTRÉAL

MÉMOIRE PRÉSENTÉ EN VUE DE L'OBTENTION

DU DIPLÔME DE MAÎTRISE ÈS SCIENCES APPLIQUÉES

(GÉNIE CHIMIQUE)

OCTOBRE 2006

Your file Votre référence
ISBN: 978-0-494-25549-0
Our file Notre référence
ISBN: 978-0-494-25549-0

UNIVERSITÉ DE MONTRÉAL

ÉCOLE POLYTECHNIQUE DE MONTRÉAL

Ce mémoire intitulé :

HYDRODYNAMICS CHARACTERIZATION OF THE MAXBLEND IMPELLER

présenté par : IRANSHAHI ARASH

en vue de l'obtention du diplôme de : Maîtrise ès sciences appliquées

a été dûment accepté par le jury d'examen constitué de :

M. BERTRAND François, Ph.D., président

M. TANGUY Philippe A., Ph.D., membre et directeur de recherche

M. PERRIER Michel, Ph.D., membre

To My Parents

ACKNOWLEDGEMENTS

I would like to express my sincere thanks and gratitude to everyone who has, in one form or another, contributed to my work in this thesis. I wish to thank:

- Professor Philippe A. Tanguy for his exceptional supervision and guidance. His suggestions and comments were always helpful and constructive.
- Doctor Mourad Heniche for his patience and his friendship. Without his help and expertise the numerical work would not have been possible.
- Doctor Louis Fradette for his kind and valuable help and guidance throughout the experimental work.
- National Science and Engineering Research Council of Canada (NSERC) for the financial support in funding this research.
- Fellow researchers at URPEI: Christphe, Francois, Stephan and Alfa for their friendly discussions and helpful suggestions.

Finally, I would like to thank my family and friends who have always encouraged and supported me in all my endeavors. This thesis is dedicated to my father, my inspiration, and to my beloved mother.

RÉSUMÉ

Les caractéristiques hydrodynamiques du Maxblend ont été étudiées dans le cas des fluides visqueux. Des expériences de laboratoire et des simulations numériques par éléments finis 3D ont été menées pour un fluide newtonien (sirop de maïs). L'étude expérimentale a permis de caractériser l'agitateur pour les régimes d'écoulement laminaire et de transition. Les variables mesurées et/ou observées sont la consommation de puissance, la décoloration, le temps d'homogénéisation et l'effet des chicanes. Les simulations numériques ont permis de prédire les champs hydrodynamiques pour différentes valeurs du nombre de Reynolds et d'effectuer l'analyse du mélange (consommation de puissance, taux de cisaillement, capacité de pompage, intensité de ségrégation et efficacité de mélange). À la lumière des résultats obtenus, pour la gamme des nombres de Reynolds étudiés dans ce travail, l'agitateur Maxblend équipé de chicanes travaille plus efficacement à la fin du régime laminaire et au commencement du régime de transition et ce en comparaison avec le scénario sans chicane.

ABSTRACT

The hydrodynamic characteristics of the Maxblend impeller have been investigated in the case of viscous fluids. Both laboratory experiments and 3D finite element based CFD simulations have been tackled for Newtonian (corn syrup) fluid. In the experimental study, the power consumption, the mixing kinetics, the mixing time and the effect of baffles in the laminar and transition flow regimes have been investigated. The numerical simulations have dealt with the prediction of the three dimensional flow patterns and the mixing performance (power consumption, shear rate distribution, pumping capacity, intensity of segregation, mixing efficiency). It is shown that in the range of Reynolds numbers studied in this work, the Maxblend mixer equipped with baffles has an efficient mixing rate within the range of end of laminar regime and beginning of transition regime.

CONDENSÉ EN FRANÇAIS

Le mélange en cuve constitue une partie importante de l'infrastructure nécessaire à la production chimique, pétrochimique et biochimique. Le succès d'un grand nombre de procédés impliquant la dissolution et la suspension des solides, la formulation des drogues, la cristallisation, des réactions chimiques, des bio-processus, etc. repose sur un mélange efficace. En dépit des applications étendues du mélange, des problèmes énormes résultent souvent d'un manque de compréhension des principes fondamentaux impliqués dans ces processus de mélange.

Dans la plupart des applications citées plus haut, le milieu révèle une viscosité élevée où les vitesses sont faibles et le régime d'écoulement laminaire. Des opérations de mélange laminaires sont généralement considérées comme inefficaces, inutiles et extrêmement coûteuses. En dépit de l'importance des applications de mélange laminaire dans l'industrie, l'information fondamentale est encore rare et n'a pas été couverte convenablement dans la littérature.

On a proposé plusieurs agitateurs pour répondre aux besoins du mélange visqueux industriel. Ils sont basées sur un agrandissement des roues à aubes ouvertes (des lames plus larges avec de grands diamètres) ou sur des conceptions à faible dégagement

comme des ancres et des rubans hélicoïdaux. Tandis que les agitateurs de proximité fonctionnent dans une plage de basses vitesses de rotation, les vitesses des agitateurs ouverts sont plutôt élevées.

L'agitateur Maxblend (Sumitomo Heavy Industries) est un agitateur large venant du Japon. Il se compose deux parties, une grande pale surmontée d'une grille. Le Maxblend est un des agitateurs les plus prometteurs de la nouvelle génération, en raison de sa bonne performance de mélange, sa faible dissipation, sa géométrie simple qui le rend facile à nettoyer et ses possibilités du fonctionnement dans une large plage de régimes hydrodynamiques (Mishima 1992 ; Kuratsu et autres. 1995). En outre, le Maxblend représente une solution de rechange intéressante aux agitateurs de proximité conventionnels et il a été employé dans plusieurs procédés.

L'objectif du travail actuel est de clarifier le comportement du Maxblend dans les régimes laminaires et de transition. Le projet considère une phase continue newtonienne en régime de mélange visqueux. Un intérêt particulier a été mis sur la performance de l'agitateur lors de la présence ou non de chicanes.

L'étude est réalisée expérimentalement et numériquement. Dans l'étude expérimentale, la puissance, la cinétique de mélange, la période de mélange et l'effet des chicanes dans les régimes laminaires et de transition d'écoulement ont été étudiés. Les simulations numériques ont traité les prévisions des modèles tridimensionnels d'écoulement et de

l'exécution de mélange (puissance d'énergie, capacité de distribution de taux de cisaillement, pompage, intensité de ségrégation, efficacité de mélange).

On a montré qu'en dépit du champ complexe d'écoulement créé par l'agitateur, le mélange homogène n'est pas atteint à de bas nombres de Reynolds et deux zones de ségrégation au fond du réservoir sont créées. En effet l'agitateur n'a pas été conçu pour cette gamme de nombres de Reynolds. Tandis que la configuration avec chicane, aux nombres de Reynolds élevés, réalise un mélange rapide et homogène, un vortex fort se crée avec la configuration sans chicane ce qui restreint l'opération aux nombres de Reynolds faibles pour cette configuration. En conclusion, les travaux réalisés permettent de recommander :

- Pour éviter le vortex et le phénomène d'entrée d'air gue, l'opération sans chicanes ne devrait pas excéder un Re=51.
- Pour réaliser l'homogénéisation complète, que la configuration avec chicane fonctionne à Reynolds supérieur à 51.

TABLE OF CONTENTS

LIST OF TABLES

LIST OF FIGURES

LIST OF APPENDICES

LIST OF SYMBOLS AND ABBREVIATIONS

Symbol	Description	Unit
a	model parameter	(-)
c	concentration	(mol/m^3)
$\overline{C}$	mean value of the concentration	(mol/m^3)
C_i	concentration in the i^{th} element	(mol/m^3)
d	impeller diameter	(m)
D	diffusion coefficient	(m^2/s)
e_λ	mixing efficiency	(-)
$< e_\lambda >$	time-averaged mixing efficiency	(-)
h	impeller height	(m)
H	tank height	(m)
K	number of elements	(-)
L_0	characteristic length	(m)
n	model parameter	(-)
n	normal vector	(-)
N	impeller speed	(rev/s)
N_t	number of time steps	(-)

N_{tracer}	number of tracers in whole domain	(-)
M	mixing evolution	(%)
M_∞	value of M at t=∞	(%)
p	pressure	(Pa)
P	impeller power draw	(W)
Q_{xy}	horizontal contribution of the flow rate	(m^3/s)
Q_V	vertical pumping or flow rate	(m^3/s)
R	tank radius	(m)
t	time	(s)
v_z^+	upward component of the velocity vector	(m/s)
v_z^-	downward component of the velocity vector	(m/s)
V_0	characteristic velocity	(m/s)
V	velocity	(m/s)
V_h^i	velocity of the i^{th} node	(m/s)
V_i	volume of the i^{th} element	(m^3)
V_{Total}	volume of the whole domain ($=\sum V_i$)	(m^3)
z	mesh size	(m)

Greek symbols

$\dot{\gamma}$	rate-of-strain tensor	(s^{-1})
λ	stretching	(-)
δ	bottom clearance	(m)
μ	viscosity	(Pa.s)
ρ	density	(kg/m^3)
τ	model parameter	(s)
ψ	stream function	(-)
ω	angular velocity	(rad/s)

Abbreviations

CFD	Computational Fluid Dynamics
DHR	Double Helical Ribbon
FFT	Fast Fourier Transform
RGB	Red-Green-Blue
SUPG	Streamline-Upwind-Petrov-Galerkin
VFEM	Virtual Finite Element Method

CHAPTER 1

INTRODUCTION

1.1 Problem statement

Mixing in agitated tanks is an important part of the infrastructure in chemical, petrochemical, and biochemical industries. The success of many processes including dissolution and suspension of solids, formulation of drugs, crystallization, chemical reactions, bio-processes, etc relies heavily on effective mixing. Despite the extensive applications of mixing, tremendous problems are very often encountered in industries due to a lack of understanding of the fundamentals involved in mixing processes. It has been estimated that 1-10 billion dollars/year are lost by North American industries due to mixing problems (Harnby et al., 1992). Most of the industries are suffering from oversimplified design of the mixing systems. While underestimated design leads to low quality of products, over design is extremely costly on large scale production plants.

In most industries dealing with food, polymer, pharmaceutical and biotechnological processing, mixing involves high viscosities medium or low rotating speeds, which means of operating at the laminar regime. Laminar mixing operations are generally considered to be inefficient, wasteful and extremely costly. Low speed laminar mixing is mainly used in biotechnological industries. Shear sensitive materials like cells require operation at low speed (Thomas, 1990). The complexity of laminar mixing problems scales when reactive systems are considered. Often the overall reaction rate, the yield of reaction, and its selectivity can achieve the desired values only when the ideal perfect mixing can be performed. More specifically, when the reaction rate is quite high, the deviation from the ideal system, can be highly influenced by performance of the mixer.

Despite the importance of laminar mixing applications in industry, fundamental information is still scarce and has not been covered properly in literature. Laminar mixing has been considered mostly as a practical art rather than a scientific challenge. Consequently, the industrial problems associated with mixing are mostly approached case by case on a trial and error basis. The lack of fundamental knowledge of mixing in laminar regime leads to inefficient mixing operations at low agitation speed or under viscous conditions.

Many industries still use open impellers like propellers, paddles and Ruston turbines, for laminar mixing operation. Not only this type of impellers is extremely inefficient for laminar regime but also they can be very damaging to microstructure in polymer

operations or to cell culture in bio-systems. Various impellers also have been proposed to respond to the needs of industrial viscous mixing. They are based either on an enlargement of open impellers (wider blades with large diameters) or on close-clearance designs like anchors and helical ribbons. While the close-clearance impellers operate in low rotational speed, the speeds of open impellers are rather high. Close-clearance impellers are designed to physically turnover the fluid, due to the difficulty of pumping viscous fluids. These impellers are typically large in size, nearly the same size as the tank diameter, and provide macro scale blending of liquid at low shear.

The Maxblend impeller (Sumitomo Heavy Industries) shown in Figure 1.1 is a wide impeller coming from Japan. It is composed of the combination of two parts, a low paddle and a grid. The Maxblend is one of the most promising impellers of the new generation, due to its good mixing performance, its low power dissipation, its simple geometry that make it easy to clean, and its capabilities of operating in a wide range of Reynolds (*Re)* numbers (Mishima 1992 ; Kuratsu et al. 1995).

The Maxblend impeller represents an interesting alternative to close-clearance impellers and it has been used in different processes. Table 1.1 shows the application of the mixer as highlighted in the SHI website (www.shi.co.jp). SHI uses the Maxblend for variety of applications in liquid-liquid, liquid-solid and gas-liquid mixing. According to the manufacturer claims, the Maxblend can handle processes from suspension polymerization and crystallization operation to high viscosity gas absorption. Although

the Maxblend has been widely used in the industry, information regarding its mixing performance is scarce.

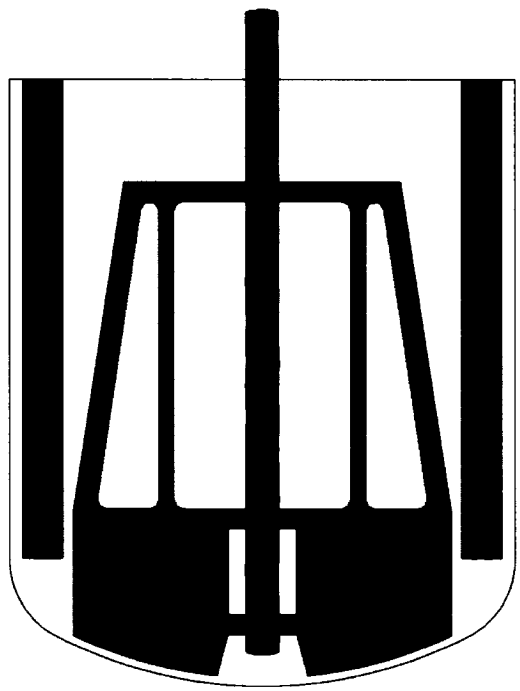

Figure 1.1 Schematic of the Maxblend.

The Maxblend design idea originally comes from multi-stage impellers. As shown in figure 1.2, the separation plan (interfering boundary) is formed by upward and downward flow while the two multi stage impellers rotating. By combining the two impellers in a wide impeller, the boundary can be eliminated. Moreover, moving the impeller close to the bottom of the tank creates just one circulation flow in the tank. Finally by adding the grid part, efficient mixing can be achieved. In addition, the simple shape of the impeller (no pitched, no angle, no spiral) makes the clean-up process easy and reduces the adhesion problem and the polymer blocks.

Table 1.1 Applications of the Maxblend mixer.

Mixing Medium	Process/Operation	Product/Application Example
Liquid-Solid Mixing	Suspension Polymerization	PVC, PS, Water Adsorbent Polymer
	Crystallization Operation	Cooling, Reaction, Condensation
	Salting-Out, Oxygenation-Out	Clam Former, ABS Precipitation
	Powder and Resin Dissolution	PVA, CMC, Lignin
Liquid-Liquid Mixing	Emulsion Polymerization	ABS, Paste PVC, Vinyl Acetate, Acrylic Emulsion
	Solution Polymerization	AS, BR, Thermoplasticity Elastomer
	Bulk Polymerization	PS, PMMA, Spandex
	Condensation Polymerization	Biodegradable Polymer
Gas-Liquid Mixing	Hydrogenation, Chlorination	Polymer Hydrogenation, Oils and Fats, Amine
	EO, PO Addition Reaction	Surfactant
	High Viscosity Gas Absorption	Thermoplastic Elastomer etc.
	High Viscosity Cultivation	Biopolymer, Bio-Cellulose

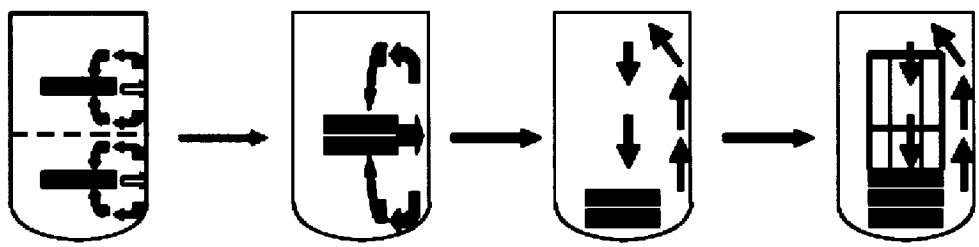

Figure 1.2 Concept of the Maxblend design

1.2 Objectives

The objective of the present work is to contribute to clarify the fluid mechanics behavior of the Maxblend in the laminar and transition regimes. The project considers single liquid phase Newtonian viscous mixing. We are especially interested in the performance characteristics of this impeller and how they compare when the impeller operates without baffle and with baffles. The study is performed both experimentally and numerically.

Here are the detailed objectives of the study:

a) Experimental study:

1. To determine the power consumption of the mixer derived from torque measurements.
2. To evaluate the mixing time and micro mixing kinetics of the Maxblend by means of discoloration technique coupled by advanced image analysis method.

b) Numerical study:

1. To simulate the flow and mixing in the tank equipped by the impeller and validate the predictions by comparison with experimental data.
2. To investigate the mixing criteria of the mixer.

1.3 Contents of the thesis

Here is a brief explanation of the following chapters of the thesis

CHAPTER 2 - Literature review:

The chapter surveys previous studies on laminar mixing and the studies focused on the Maxblend mixer performances. The chapter also has a brief review on application of CFD on stirred tank reactors mixing.

CHAPTER 3 - Overall methodological approach:

This chapter starts by describing the experimental setup and materials. Then, it explains the overall methodology for both experimental and numerical studies.

CHAPTER 4 - Hydrodynamics characterization of the Maxblend impeller

This chapter presents the article.

CHAPTER 5 – Additional results

The chapter consists of the addition experimental and numerical data that for brevity are not included in the article.

CHAPTER 6 – Conclusion and recommendations

APPENDIX A – Computational procedure for pumping capacity

This appendix consists of the mathematical procedure for pumping computation and explains how it is used for agitated tank applications.

CHAPTER 2

LITERATURE REVIEW

2.1 Laminar mixing

Many mixing applications involve fluids of varying viscosity, stirred under laminar flow conditions, where knowledge of the local and overall flow pattern as well as shear stress distribution is very important. While most studies have concentrated on turbulent flow in mixing vessels, there are many industrial applications involving highly viscous fluids or requiring very slow mixing rates. These applications necessarily operate in the laminar flow regime where mixing is often inefficient due to the presence of segregated regions. Thus, extreme care must be taken in the design of these systems.

There are several studies that primarily focus on the characterization of the chaotic nature of mixing processes in laminar flows as opposed to the detailed investigation of the flow field. For example, Alvarez et al. (2002) studied the chaotic nature of the flow

in mixing vessels equipped by multi stage impellers for *Re* in the region 20–80 and found that 98% of the power expended in mechanical stirring produces no detectable mixing at all, and in fact convective mixing is generated solely by tiny perturbations to a dominant non-chaotic flow.

For highly viscous fluids, helical ribbon, screw and anchor impellers provide an alternative to the standard turbine impellers (Bakker and Gates, 1995). De la Villeon et al., (1998) found out close clearance impellers such as helical ribbons have a good mixing performance in laminar regime. Noting that the two types of impellers can be combined, Tanguy et al. (1997) studied the mixing performance of a dual impeller composed of a disc turbine and helical ribbon impeller. They conclude that the new configuration outperform the standard helical ribbon when the rheology evolves. A coaxial mixer composed of an anchor impeller as well as a series of rods and a pitched blade turbine was also studied experimentally and computationally by Thibault and Tanguy (2002).

2.2 The Maxblend mixer

The Maxblend impeller represents an interesting alternative to close-clearance impellers and it has been used in different processes as highlighted in the SHI website. However, information is pretty scarce on the reasons explaining its good performance. Hiruta et al.

(1997) investigated the application of the Maxblend fermentor for microbial processes and compared its performance with turbine impeller fermentor. They concluded that since shear stress distribution for the Maxblend is more uniform than turbine impeller. A study also carried out on effect of the Maxblend and four other impellers on bacterial cellulose productivity in aerated and agitated culture (Kouda et al. 1997). Saito et al. (1999) compared performance of the Maxblend with five other impellers on biotin production. They concluded that turbine blade impeller is more suitable for this application. A numerical investigation on dispersive mixing of the Maxblend and a comparison with helical ribbons impellers has also been carried out (Yao et al. 2001). They found that although the Maxblend has efficient performance at high Reynolds numbers, the dispersive mixing cannot be achieved at deep laminar regime. Sumi and Kamiwano (2001) have investigated some mixing characteristics of the Maxblend with highly viscous fluids and compare it with multistage impellers. Power consumption and solid suspension performance of the Maxblend and other large-scale impellers in gas-liquid-solid reactor were investigated by Dohi et al. (2003). They found out the Maxblend has the minimum power consumption and the most uniform solid suspension among the large scale impellers. Finally, liquid phase mixing time in boiling stirred tank reactors for the Maxblend and other large scale impellers were investigated by Takahashi et al. (2006a), who found that the Maxblend has essentially the same performance as competing impellers in this application.

2.3 Application of CFD on stirred tank reactors mixing

CFD is the science of predicting fluid flow, heat transfer, mass transfer, chemical reactions, and related phenomena by solving the mathematical equations that govern these processes using a numerical algorithm on a computer. Computational fluid dynamics (CFD) programs were first developed in the 1960s; they were however severely restricted due to the limited computing power in those days (Bakker et al., 2001). It was not until the early 1980s that commercial codes became available, mainly because of the spectacular progress in digital computing in the past two decades. The application of CFD to stirred tank reactors dates back to the late 1970s (Harris et al., 1996).With the advances in computing power together with modern methods, CFD has reached a level that gives reliable and accurate results for applications involving single flow stirred tank reactors (Bartels *et al.*, 2002).

Several methods have been successfully developed to simulate the flow in a stirred vessel, where good agreement of the flow field with experimental data was achieved. With the ever decreasing computing costs and the continuous development of commercial codes for CFD, the simulation of three-dimensional flow fields in a stirred vessel is increasingly gaining acceptance as an alternative to the traditional modeling approaches. The use of computer simulations to investigate the dynamics of agitation in stirred vessels is now well established in the laminar and turbulent regimes. Several

articles dealing application of CFD on stirred tank mixing performance can be found in the literature in the laminar regime (e.g. Tanguy et al., 1992; De La Villéon et al., 1998).

The particular challenge of numerical simulation lies in the relative motion between stationary baffles and the rotating impeller, resulting in the flow domain changing with time. Numerous approaches have been proposed for this type of problems, among them are the virtual finite element method (VFEM) by Bertrand et al. (1997). VFEM has successfully been applied to simulate the unsteady behavior of impeller regarding to the baffles.

CHAPTER 3

OVERALL METHODOLOGICAL APROACH

3.1 Experimental setup and materials

The Maxblend configuration (Figs 1.1 and 3.1) considered in this work consists of a vessel of 2 liters in volume. A variable speed motor drives the Maxblend, which speed is being carefully controlled by a solid-state frequency variator, receiving a feedback signal from a speed encoder. A rectangular transparent chamber surrounds the tank to minimize optical distortions effects due to the curvature of the tank. The system is equipped by elevator to help moving of the impeller to adjust the position of the impeller.

The power consumption of the impeller is derived from torque measurements obtained from torque meter. Two different torque meters were utilized, one ranging from 0-500 N.m, the other from 0-20 N.m. Both torque meters were carefully calibrated before the experimental runs.

Figure 3.1 Experimental setup

Newtonian fluid (glucose syrup) was used, which enables to adjust the viscosity by diluting the medium with water. Finding the optimum viscosity was a challenging task, since the bulky shape of impeller causes significant viscous dissipation at a viscosity above 8 Pa.s. . Viscous dissipation increases the temperature of the tank and decreases the glucose viscosity very sharply, consequently making the experimental measurements

hardly accurate. On the other hand, with the limited range of rotational speed of the motor drive (0 to 120 rpm), it was difficult to find a viscosity to operate the system from deep laminar to the transition regime without changing the medium. In practice, the value of the viscosity μ was adjusted to 5 Pa.s with a density ρ of 1279 kg/m^3, allowing *Re* values between 0 and 100.

3.2 Experimental methods

Experiments consisted of two parts, the power measurement of impeller and mixing time and kinetics measurement. Mixing time and kinetics were evaluated in two steps, (*i*) by means of discoloration technique base on fast acid-alkaline indicator (Lamberto et al. 1996); (*ii*) by analyzing the images taken with advanced image analysis method (Cabaret et al. 2006).

During discoloration experiments, the temperature was monitored by a thermocouple thermometer with an accuracy of 0.1 °C to avoid the effect of viscous dissipation. The significant viscous dissipation heat caused by the bulky shape of impeller decreases the viscosity of glucose syrup as a very thermally sensitive medium. Therefore, the value of viscosity is corrected based on the variation of temperature.

3.3 Numerical methods

The fluid flow generated in the Maxblend mixer is governed by the classical momentum and mass conservation principles. To numerically predict the three-dimensional flow pattern in a stirred tank, two formulations of the Navier–Stokes equations can be established depending whether the Eulerian viewpoint or the Lagrangian viewpoint (Figure 3.2) is used. In Lagrangian viewpoint, the impeller is fixed and the tank is rotating. Although the Lagrangian viewpoint could simply be considered for the unbaffled mixer configuration, a special procedure was required to address the complexity of the impeller kinematics for the baffled configuration. Therefore, the Eulerian frame of reference was used to reproduce the unsteady position of the impeller regarding to baffles. For comparison reasons, we also decided to simulate unbaffled configuration in the same fashion as baffled configuration, over the time in Eulerian view point. All the computations performed by using a finite element method similar to that described in Tanguy et al. (1992). The virtual finite element method (VFEM) approach (Bertrand et al.,1997) was used to simulate the unsteady behavior of the Maxblend.

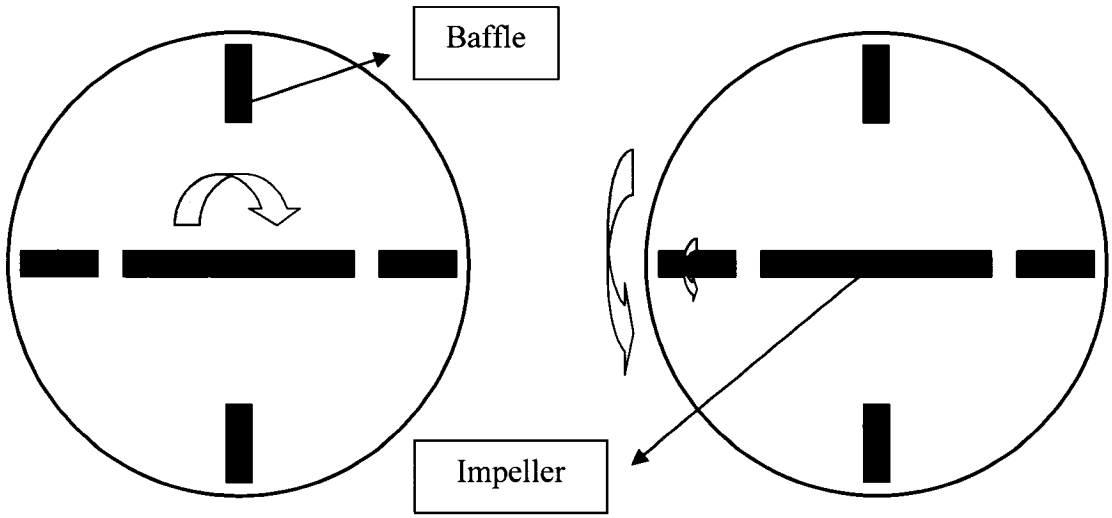

Figure 3.2 Comparison of Eulerian and Lagrangian viewpoint.

In order to better understand the transport phenomena of mixing mechanism involved in discoloration technique, mass transfer equations for acid and alkaline should be solved. Mass transport phenomena of mixing consist of two terms, convection and diffusion. Numerical solution of the mass transfer equation can be challenging, due in part to the mixed hyperbolic–parabolic nature of the equation. Spurious oscillations in the solution are generated, particularly in regions of high gradients mainly when the acid is just injected. Numerous approaches have been proposed to preclude oscillations in advection-diffusion transport problems, regardless of mesh or time step refinement. Among them are streamline-upwind/Petro-Galerkin (SUPG) formulations (Hughes and Brooks, 1982; Brooks and Hughes, 1982; Tezduyar et al., 1987) that has successfully been applied to various problems governed by convection-diffusion phenomena. In this

work we use a SUPG-base finite element formulation for this time-dependent convection-diffusion problem. The transport equations are given in detail in the next chapter.

The spurious oscillations especially at high Peclet number can corrupt the whole solution, therefore, a numerical constraint in terms of maximum value of feasible Peclet exists for the solution of convection dominated problems. Table 3.1 shows the effect of different Peclet numbers on minimum and maximum value of concentration at t= 1 s. It should be noted the experimental value of concentration varies from 0 to 200 mol/m^3. The table illustrates the maximum oscillating behavior of the system, since when the acid is just injected, the maximum regions of high gradients exist in the solution. Although the order of experimental Peclet number is higher than 10^6, as showed in the table we could not go farther than Pe=1000 in this study. In addition, the negative values of the concentration at this specific Peclet, Pe=1000, corresponds to a limited number of nodes mainly in very high gradients regions at the beginning of mixing process. The oscillation in this case disappears after 10 rotations of the impeller. The table also shows the effect of SUPG formulation at Pe=1000, apparently SUPG has great influence on reducing the oscillation.

Table 3.1 Effect of Peclet number on oscillating behavior of the solution at t=1 s

Pe	Cmin	Cmax	SUPG
1×10^{2}	-5.28	91.6	ON
1×10^{3}	-19.72	175.79	ON
1×10^{3}	-51.28	205.71	OFF
1×10^{4}	-4.32×10^{65}	8.64×10^{65}	ON
1×10^{5}	-687970	42198	ON
1×10^{6}	-636.6	1499.6	ON
1×10^{7}	-2391	10404	ON

The finite element method requires the generation of a computational mesh. In the present work, I-DEAS (EDS) software was used. Mesh generation is an important part in any finite element numerical simulations. I-DEAS enables to divide the geometry of the main volume into one or several congruent volumes. Partitioning can be used to prescribe a specific mesh size to each volume, so that a mesh with variable finite element densities can be generated. Depending on the needs, it is then possible to refine the mesh in the regions of interest, for instance where high shear rates are present, and relax the mesh size elsewhere. Different non-uniform meshing strategies were

investigated. A fine mesh was generated close to the baffles and the impeller and in the bottom gap between the impeller and the tank walls where the highest shear rates are produced. A coarser mesh was used in the other regions of the vessel.

The simulations were performed in all cases with commercial 3-D finite element software POLY3D™ (Rheosoft), which uses an efficient Krylov-based Uzawa solver (Bertrand and Tanguy, 2002).

CHAPTER 4

HYDRODYNAMICS CHARACTERIZATION OF THE MAXBLEND IMPELLER

Arash Iranshahi[1], Mourad Heniche[1], Louis Fradette[1], Philippe A. Tanguy[1] and Katsuhide Takenaka[2]

[1] *URPEI, Department of Chemical Engineering, Ecole Polytechnique*

P.O. Box 6079, station CV, Montréal (Québec), H3C 3A7, Canada

[2] *SHI Mechanical & Equipment Inc., Ehime, Japan*

Key Words:

Maxblend, fluid mixing, Computer simulations, finite element method

Submitted: Chemical Engineering Science (September 2006)

4.1 Abstract

The hydrodynamic characteristics of the Maxblend impeller have been investigated in the case of viscous Newtonian fluids. Both laboratory experiments and 3D finite element based CFD simulations have been carried out. The power consumption, the mixing kinetics, the mixing time and the effect of baffles in the laminar and transition flow regimes have been determined. It was found that in the range of Reynolds numbers studied in this work, the best window performance of the Maxblend mixer is the end of the laminar regime and the early transition regime with baffles.

4.2 Introduction

Mixing of viscous fluids is mainly carried out in the laminar and transition regimes. When standard open impellers are used, it is often associated with poor bulk motion, an inhomogeneous distribution of the various phases, and the presence of spurious rheologically-induced phenomena such as caverns. In the laminar regime, mixing is obtained by sequences of stretching-folding-breaking mechanisms of the secondary phase and not by highly energetic eddies, making the design of optimal mixers very challenging.

Various impellers have been proposed to respond to the needs of laminar viscous mixing. They are based either on an enlargement of open impellers (wider blades with large diameters) or close-clearance designs like anchors and helical ribbons. The Maxblend impeller (Sumitomo Heavy Industries) shown in Figure 4.1 is a wide impeller that combined a lower paddle and a grid. The Maxblend is claimed to be one of the most promising impellers of the new generation, due to its good mixing performance, its low power dissipation, its straight geometry that makes it easy to clean, and its capabilities of operating in a wide range of Reynolds number (*Re*) (Mishima 1992 ; Kuratsu et al. 1995).

Detailed information regarding the Maxblend performance is limited. Sumi and Kamiwano (2001) have investigated some mixing characteristics of Maxblend with highly viscous fluids and compare it with multistage impellers. A numerical investigation on dispersive mixing of the Maxblend and a comparison with helical ribbons impellers has also been carried out (Yao et al. 2001). They concluded that in deep laminar regime, the Maxblend cannot reach an effective dispersive mixing. The Maxblend power consumption and solid suspension performance in gas–liquid–solid applications were also investigated and compared with other large-scale impellers (Dohi et al. 2004). They found out that the Maxblend creates a more uniform solid suspension in comparison to Fullzone and triple impellers. The mixing performance of Maxblend and other large impellers in boiling stirred tank reactors was investigated by Takahashi et al. (2006a), who found that the Maxblend has essentially the same performance as the

other impellers in this application. Numerical and experimental comparisons of Maxblend with double helical ribbon (DHR) were carried out by Takahashi et al. (2006b). They concluded that although Maxblend and DHR have almost the same power consumption, Maxblend has longer mixing time where $Re<10$ and shorter where $Re>10$.

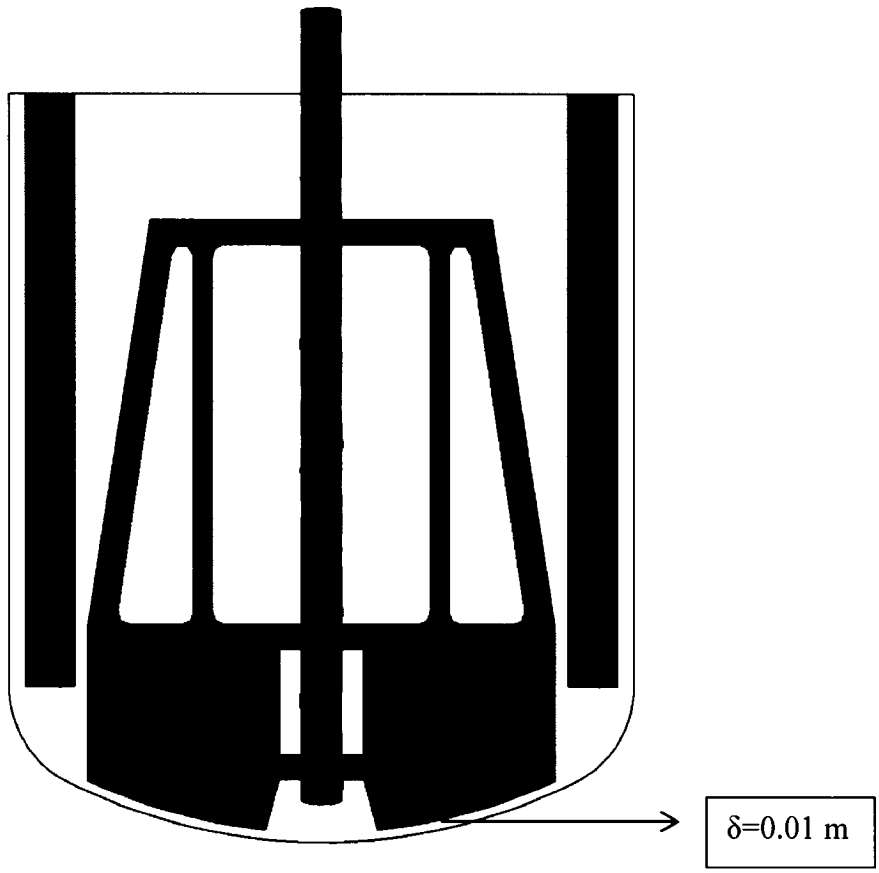

Figure 4.1 Schematic of the Maxblend.

The use of computer simulations to investigate the dynamics of mixing in stirred vessels is now well established in the laminar and transition regimes. Several articles dealing with close-clearance impellers can be found in the literature (e.g. Tanguy et al. 1992; De La Villeon et al. 1998; Iranshahi et al. 2006). For a long time, the mixing in laminar regime was examined without consideration of the concentration profile. Among the working hypothesis, it was assumed that the diffusion had no effect on the laminar mixing and the mixing was governed only by bulk transfer. Consequently the mixing system simulation consisted of only the flow equations regardless of any mass transfer phenomena involved in the mixing. In the present study, mass conservation with momentum conservation has been considered to better understand the mixing mechanisms of the Maxblend mixer.

The objective of the present work is to characterize experimentally and numerically the Maxblend mixer in the laminar and transition regime with Newtonian fluid. Experiment consists of two parts namely the power measurement of the impeller and mixing time and kinetics measurement. In addition, CFD simulations are also performed, which comprise two steps: (*i*) a validation step involving the comparison of the predictions versus experimental data; (*ii*) the investigation of mixing criteria and comparison of the results obtained for baffled and unbaffled configurations.

4.3 Methodology

4.3.1 Experimental setup and methods

The Maxblend configuration is shown in Figure 4.1. It consists of a vessel of diameter *D* 600 mm and a liquid height *H* of 720 mm. The Maxblend impeller has a diameter *d* of 450 mm and a height *h* of 600 mm and is driven by a variable speed motor. The speed is carefully controlled by a solid-state frequency changer, receiving a feedback signal from a speed encoder. In addition, the shaft is equipped with a torquemeter to measure the effective power consumption of the impeller. The tank can be equipped with four equally spaced baffles of 50 mm wide. In this work two mixing configurations are studied: unbaffled configuration and baffled configuration.

A Newtonian glucose syrup aqueous solution having a viscosity μ of 5 Pa.s and a density ρ of 1279 kg/m^3 was used as the working fluid. The temperature was carefully monitored to control the significant viscous dissipation caused by the bulky shape of impeller and correct the viscosity value in the result analysis accordingly, as glucose syrup is a very thermally sensitive medium.

Mixing times and kinetics were evaluated by means of discoloration technique based on a fast acid-alkaline indicator reaction (Lamberto et al. 1996). The tracer solution was prepared with 0.08 % bromocresol purple as an indicator in water. A volume of 900 mL

of this solution was mixed with a 900 mL of aqueous corn syrup, added to the tank and thoroughly mixed. Subsequently, a solution consisting of 1000 mL of aqueous corn syrup and 20 mL of 10 N NaOH was added and solution was mixed until a uniform purple color was observed. Then, the mixer was stopped and 1000 mL of aqueous corn syrup and 20 mL of 10 N HCl was added at time zero and mixed until a uniform yellow color was observed corresponding to the mixing time. For comparison purposes between the different operating conditions, this solution was always added at the same injection point at the free surface close to the shaft. Mixing times were measured only from the alkaline state to the acidic state, since the visualization of the color change from purple to yellow is much easier to distinguish than from yellow towards purple. The fluid viscosity measurement as well as the mixing experiments were performed at lab temperature (~23 °C).

Advanced image analysis method (Cabaret et al., 2006) was used to determine the macro-mixing kinetics of the impeller. The technique consists of capturing a video during the color change and using image analysis for the quantification of the degree of macro-mixing and mixing time.

For video capturing, a rectangular transparent chamber surrounding the tank was installed and filled with water to minimize optical distortions effects due to the curvature of the tank. White sheets of paper were used as light diffuser on the rectangular vessel. The mixing process was recorded by a digital camera at 25 frames per second and the

captured images were sampled when the impeller was perpendicular to the camera. From each mixing time recorded, 200 pictures were collected and the images were analyzed by using Image-Pro Plus v.4.5.1 (Media Cybernetics) software to determine the mixing kinetics.

4.3.2 Numerical methods

We adopted the Eulerian viewpoint for the flow description (Bertrand et al., 1992). In this frame of reference, the flow equations are expressed as follows:

$$\rho\left(\frac{\partial V}{\partial t} + V\,\text{grad}\,V\right) + \text{grad}\,p - \text{div}\left(2\mu\left(\dot{\underline{\underline{\gamma}}}\right)\dot{\underline{\underline{\gamma}}}\right) = 0 \qquad (4.1)$$

$$\text{div}V = 0\,. \qquad (4.2)$$

In (4.1), $\dot{\underline{\underline{\gamma}}} = (1/2)[\text{grad}V + (\text{grad}V)^T]$ is the rate-of-strain tensor, $V(V_X, V_Y, V_Z)$ the velocity vector, and p the pressure. The free surface is assumed to be flat and horizontal. The boundary conditions are:

- At the vessel wall and bottom and baffles surface: $V = 0$;
- At the free surface: $V_z = 0$;
- On the impeller: $r = r(t), V(t) = \omega \times r(t)$.

where $r(t)$ is the time-dependent radial coordinate and ω the angular velocity. The fluid is supposed at rest at $t = 0$.

The virtual finite element method (VFEM) approach (Bertrand et al., 1997) was used to simulate the unsteady behavior of Maxblend. This approach is based on the imposition of the impeller kinematics by means of a set of control points distributed along the surface of the impeller. At each time step, the velocity and position of the control points is updated and a new problem is solved. This method is a particular type of fictitious domain method (Glowinski et al., 1994) and was specifically developed for the analysis of flow problems in enclosures containing internal moving parts like mechanically agitated mixers. A total of 12 time steps for the Maxblend were calculated for one revolution of the impeller.

In order to better understand the mixing mechanism involved in discoloration technique, the convective-diffusive mass transfer equations for acid and alkaline should be solved. A basic mass transport phenomenon of mixing consists of two terms, convection and diffusion. Due to the binary character of mass conservation of titration process that consists of only one acid and one base, a single mass conservation equation is sufficient for the modeling of the physical problem. In this work, we solved the dimensionless form of the governing equation for mass convection–diffusive transport of the acid:

$$\frac{\partial c}{\partial t} + V \text{ grad } c = \frac{1}{Pe} \text{ div } (\text{ grad } c\ ) + f \tag{4.3}$$

where c is the acid concentration, V is a known velocity field, $Pe = V_0 L_0 / D$ is the Peclet number (D is the diffusion coefficient, and V_0 and L_0 are characteristic velocity and length scales), and f represents kinetics reaction terms.

Numerical solution of Eq. (4.3) can be challenging, due to the mixed hyperbolic–parabolic nature of the equation that requires a careful choice of the numerical scheme. For diffusion dominated cases, the standard Galerkin finite element approach works well, and fairly reliable results can be achieved. When convective effects dominate, (high Pe values), the Galerkin method generates spurious oscillations, particularly in regions of high gradients, in our case where the acid is injected. Although these spurious oscillations degrade the whole numerical solution, they can be controlled by space and time discretization refinement, which is a costly procedure. Several numerical schemes have been proposed to prevent these well known unphysical oscillations in advection dominated transport problems. One of the most popular within the finite element framework is the Streamline-Upwind Petrov-Galerkin (SUPG) scheme (Hughes and Brooks, 1982; Brooks and Hughes, 1982; Tezduyar et al., 1987) that has successfully been applied to various problems governed by convection-diffusion phenomena. In this paper, the SUPG-Gear space-time formulation was used to solve the time-dependent partial differential convection-diffusion equation governing the acid mass transfer

phenomena. Finally, since the titration is an extremely fast reaction, the equation of changes in discoloration technique are mainly controlled by mass transfer only and not reaction, therefore the reaction term f in Eq. (4.3) can be eliminated.

Eq. (4.3) was solved subjected to the following Neumann boundary condition:

- at any surface $\partial\Omega$ of the domain Ω : $\left.\frac{\partial c}{\partial \mathbf{n}}\right|_{\partial\Omega} = 0$.

where $\mathbf{n}$ is the outward normal unit vector. The initial condition for the time dependent concentration profile was similar to the experiments, i.e. one liter of a mixture of glucose syrup and 20 cc of 10 M acid hydrochloric is injected at the top surface of the tank, representing the initial value of 200 mol/m^3 acid concentration. The initial value of concentration elsewhere in the tank was set to be zero.

The selection of an appropriate time step is another challenging task for convection dominated problems. The time step must be small enough to stabilize the scheme and avoid the oscillations but at reasonable computational cost. In this work, we used the correlation purposed by Zienkiewicz and Taylor (2000) which allows the estimation of the time step based on the value of the local Peclet number:

$$\frac{V_{element}\,\Delta t}{z} \leq \sqrt{\frac{1}{Pe_{element}^{\,2}} + 1} - \frac{1}{Pe_{element}} \qquad (4.4)$$

where $V_{element}$ is the element velocity, z mesh size, $Pe_{element}$ element Peclet number and Δt the time step. In practice, the time step was adjusted to 0.01 s in the all of computations.

The solution of the mass transfer equation requires the transient velocity field as an input data. In order to accelerate computational procedure, a Fast Fourier Transform (FFT) method (Cooley and Tukey, 1965) was implemented which consists of approximating the transient velocity as follows:

$$V_h^i(t) = \alpha_0^i + \alpha_m^i \cos(mt) + \sum_{k=1}^{m-1} \left(\alpha_k^i \cos(mt) + \beta_k^i \cos(mt)\right) \tag{4.5}$$

where V_h^i is the computed velocity on the i^{th} node of the grid and t is the time component. On the right hand side of (4.5), α_k^i and β_k^i are the corresponding components of the FFT and m is the number of harmonics. For time periodic flows like that generated by the Maxblend mixer, the number of harmonics can be approximated by $m=N_t/2$, N_t is the number of time steps to cover a period (N_t=12 in this study).

I-DEAS (EDS) software was used to generate the computational mesh required by the finite element method. Different non-uniform meshing strategies were investigated. A fine mesh was generated close to the baffles and the impeller and in the bottom gap

between the impeller and the tank walls where the highest shear rates are produced. A coarser mesh was used in the other regions of the vessel.

The non-uniform mesh used for baffled and unbaffled configurations simulations comprised 200,000 and 130,000 linear P_1^+-P_0 tetrahedral elements respectively (Bertrand et al., 1992). A linear system of 1,400,000 velocity-pressure equations and 40,000 concentration equations was solved for baffled configuration while the number of velocity equations and concentration equation for the unbaffled configuration were 940,000 and 24,000 respectively.

The simulations were performed in all cases with commercial 3-D finite element software POLY3D™ (Rheosoft), which uses an efficient Krylov-based Uzawa solver (Bertrand and Tanguy, 2002). All computations were performed on an IBM p690 computer. Graphical post-processing of the results was performed with Ensight (CEI).

4.4 Results and discussion

4.4.1 Power consumption

In mixing, the flow regime is characterized by the Reynolds number, *Re*, defined in agitated tank as:

$$\mathrm{Re} = \frac{\rho N d^2}{\mu} \tag{4.6}$$

where d is the impeller diameter and N is the rotational speed. The power consumption is classically represented by the dimensionless power number N_P as follows:

$$N_p = \frac{P}{\rho N^3 d^5} \tag{4.7}$$

where P stands for the power and d is the impeller diameter. In the laminar regime, the power constant $K_P = N_p.\mathrm{Re}$ is often used to compare different impellers.

Figure 4.2a-b present the numerical and experimental power consumption data for both baffled and unbaffled configurations. The experimental K_p value for the unbaffled configuration is 190. When baffles are added, the power consumption increases by an amount of 15 % (K_p=218). The experimental data are in very good agreement with the mixing theory that at very low *Re* (laminar regime) the master power curve (*Np* vs. *Re*) has a slope of −1. In addition, the value of the critical Reynolds number where the transition regime starts is approximately 25 and 38 for baffled and unbaffled configurations respectively. The agreement between numerical results and experimental

data is excellent. The discrepancy between the experimental and numerical value of K_p for unbaffled and baffled configurations is 4 % and 9 % respectively.

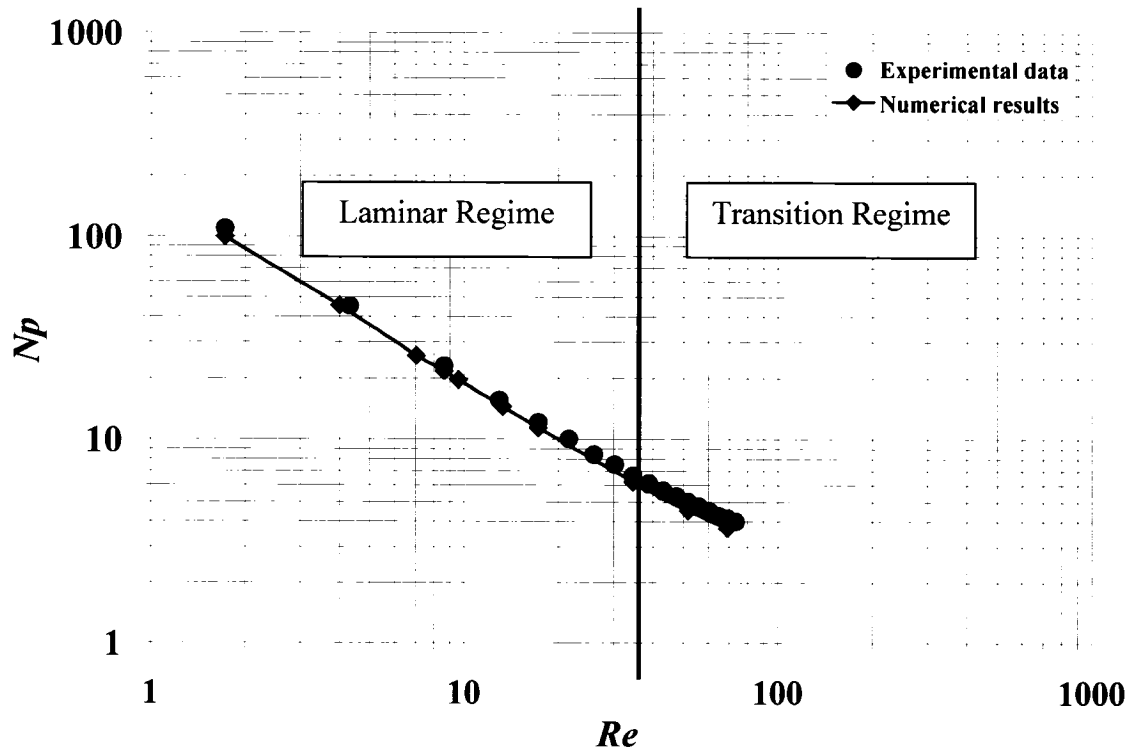

Figure 4.2 (a) Numerical and experimental power consumption data for unbaffled configuration.

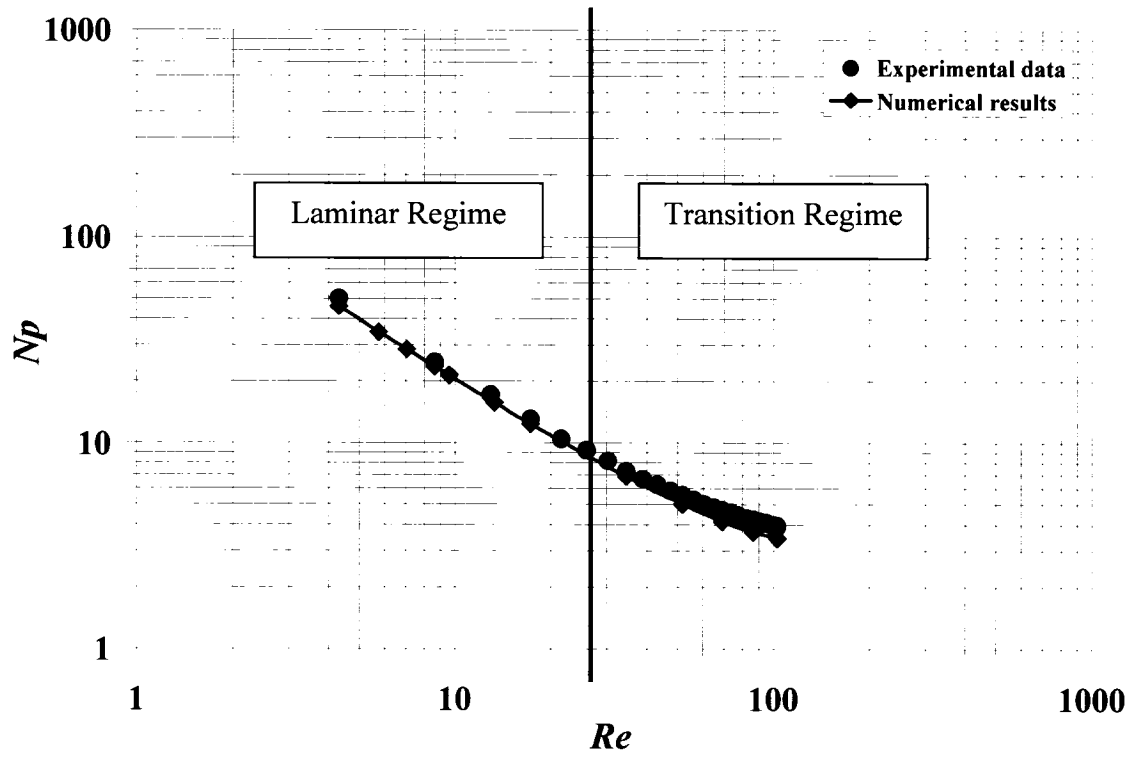

Figure 4.2. (b) Numerical and experimental power consumption data for baffled configuration.

4.4.2 Flow patterns

Figures 4.3-4.4 show the computed streamlines pattern and the axial velocity field in elevated surface respectively for the unbaffled configuration. The paddle at the vessel bottom produces a strong tangential flow and a weak axial flow, generating a strong recirculation at the vessel bottom that causes flow segregation. Above the paddle, the grid part generates an axial pumping, with an upward motion at the vessel wall and a

downward flow along the shaft. Four large vertical laminar loops exist in the vessel (Figure 4.3), two near the paddle (one in front and one behind) and two in the grid region. In fact, due to the symmetry, these four loops comprise two mixing structures: one at the bottom and one at the grid part. For the sake of brevity, we will refer to these two structures as paddle structure and grid structure. It should be noted that the flow pattern for the baffled configuration is similar to the unbaffled one, except in the vicinity of the baffles where the velocity is close to zero. Figure 4.3 also illustrates the effect of Reynolds number on the mixing structure. It appears that as the Reynolds increases, the volume of the paddle structure decreases.

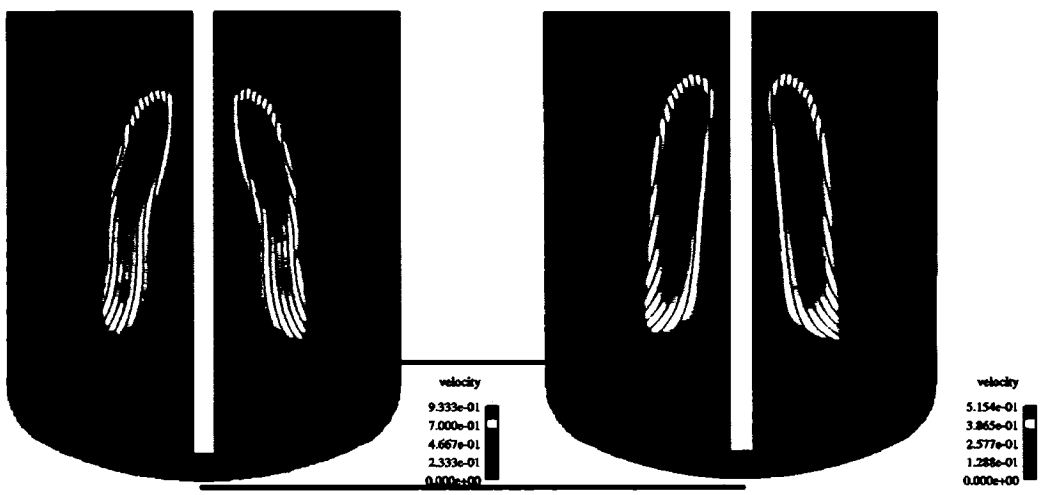

Figure 4.3 Effect of Reynolds numbers on streamlines and velocity field for unbaffled configuration.

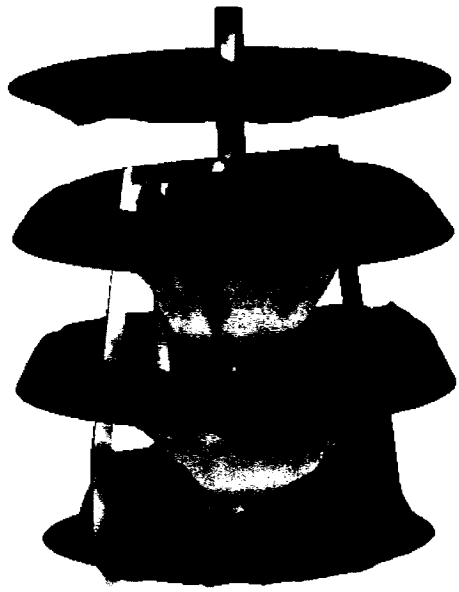

Figure 4.4 Contour of the axial component of the 3D velocity field for Unbaffled configuration (Re=60).

4.4.3 Shear rate distribution

The shear rate in a mixer is a key parameter controlling disperse mixing. In some applications where deformation and breakup of bubbles, droplets, particle agglomerates, and biological cells are involved, the local shear rate distribution must be determined (Thomas, 1990).

Figure 4.5a-b show the absolute value of the local shear rate vs. the tank radial coordinate, at four different tank heights H for unbaffled and baffled configurations at *Re*=51. Obviously, the baffled configuration creates more shear rate variations in the tank. At H=0.1 m both configurations have the maximum shear rate at the impeller external edge (R=0.25 m). This height corresponds to the paddle part of the impeller, where the interaction between the paddle edge and the baffle increases the shear rate by 30 % compare to the unbaffled configuration. At H=0.3 m, corresponds to the grid part of impeller where the radius of the impeller decreases with increased height, both configurations have again the maximum shear rate at the external edge of the impeller (R=0.2 m). The distance between the impeller and the baffles is wider in the grid region compared to the paddle part and there is almost no interaction between impeller and the baffles, therefore the shear rate close to the baffle (R=0.25 m) is minimum. H=0.6 m corresponds to the top clearance where both configurations have almost uniform shear rate distribution. Again, the shear rate is minimum around the baffle (R=0.25 m).

As mentioned before, a very close clearance exists between the impeller and the bottom of the tank (δ= 0.01 m) that causes a significant interaction between these two parts (Figure 4.1). For both configurations, the gap is the tank region where on average the shear rate is the highest (Figure 4.5a-b). The peak value of the shear rate is located at the corner edge of the impeller as expected. In conclusion, compared to blade turbine impellers (Wue et. al., 2006), the Maxblend has a very uniform shear rate distribution that makes it suitable for many shear sensitive processes.

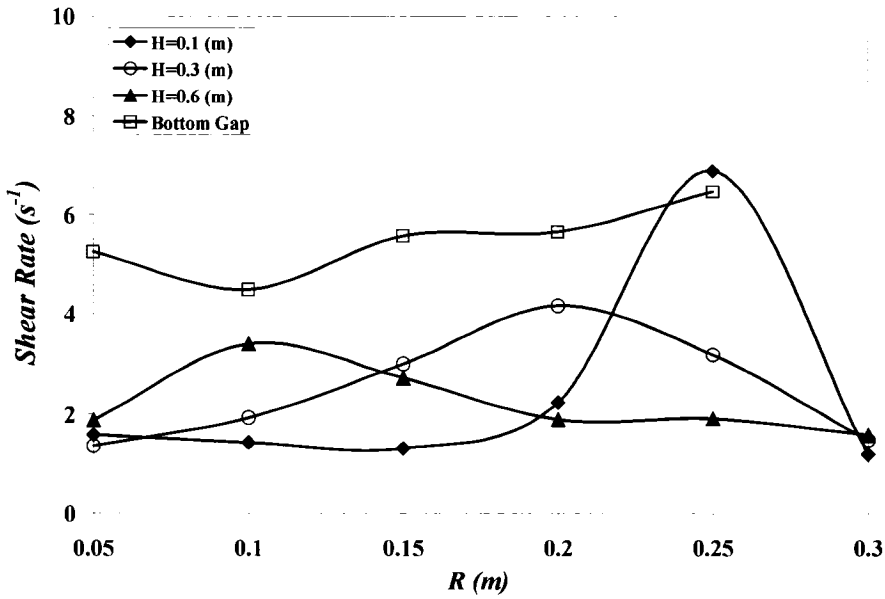

Figure 4.5 (a) Local shear rate vs. tank radius, along the tank height for the unbaffled configuration (*Re*=51).

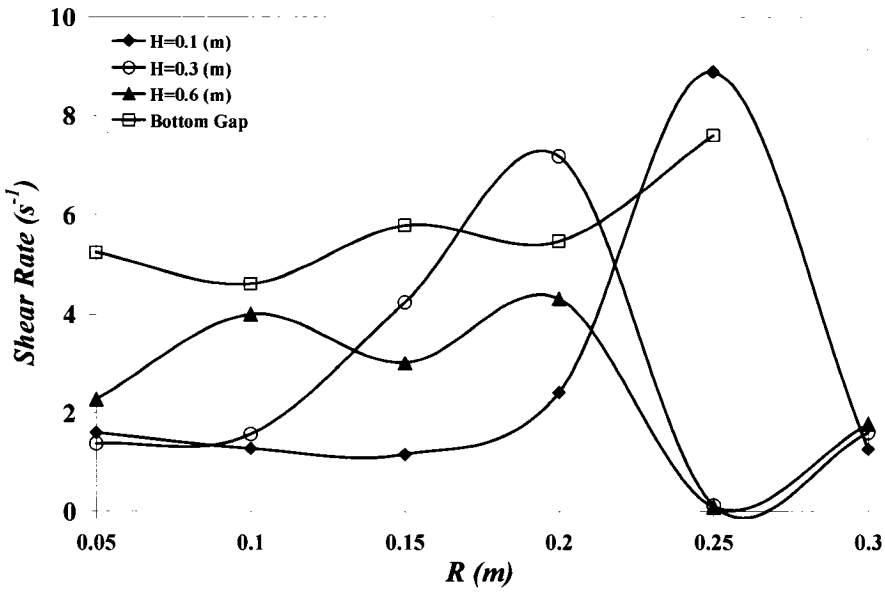

Figure 4.5 (b) Local shear rate vs. tank radius, along the tank height for the baffled configuration (*Re*=51).

4.4.4 Pumping capacity

The assessment of the pumping capacity of the Maxblend impeller was performed following the method of Iranshahi et al. (2006). A set of 14 horizontal planes was considered across the tank height. Table 1 shows the axial flow numbers N_q and percentage of different components of pumping for the two configurations, where

$$N_q = \frac{Q_V}{Nd^3} \tag{4.8}$$

In the range of Reynolds number investigated in this study, the flow numbers are almost constant. The presence of baffles increases the axial pumping and the flow number for the baffled configuration is higher than with the unbaffled configuration. The data of Table 1 confirms that the pumping of impeller is mostly axial. For the configurations under study, the pumping capability in the tangential direction is much stronger than that in the axial direction, which is a typical mixing behavior for viscous fluids.

Figure 4.6 shows the up-pumping flow rate along the impeller height for unbaffled configuration at *Re*=40. The paddle part and the top clearance have the minimum axial flow rate value. The main axial pumping in the tank appears in the grid region. The pumping curve for the baffled configuration is similar to that of the unbaffled configuration and is not shown here.

Table 4.1 Numerical comparison of axial flow number and percentage of different components of pumping for both configurations.

	Unbaffled	Baffled
Nq	0.16	0.21
Axial %	12	20
Radial %	6	7
Tangential %	82	73

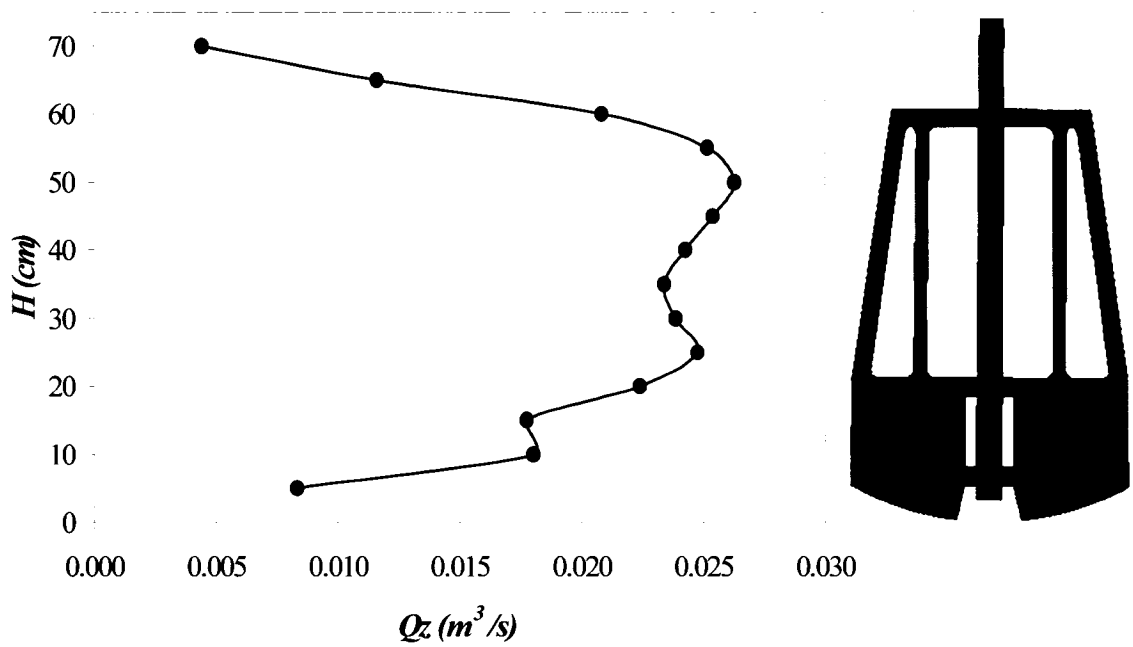

Figure 4.6 Axial pumping along impeller height for unbaffled configuration (Re=40).

4.4.4 Discoloration technique

Figures 4.7a-c show a series of experimental photos of the discoloration process and predicted concentration profile for the baffled and unbaffled configurations at *Re*=34. The numerical results consist of two vertical and horizontal mid-height cutting planes showing the concentration field. Unfortunately, the pictures (a 2D view of a 3D phenomenon) cannot be strictly compared to the numerical results. The numerical results help to better understand the mixing mechanism that cannot be visualized by experiment, especially at the beginning of the mixing process when the purple color of alkaline phase makes it impossible to visualize the mixing process within the tank. These figures reveal how the acidic fluid invades the tank and shows the location of the two little segregated zones at the bottom of the tank for both configurations, as predicted by numerical simulation (Figure 4.3).

Figure 4.7a shows the concentration profile after 9 s. The two configurations exhibit almost the same mixing mechanism during this period. The acid starts to diffuse around the injection point by forming an arms-like structure.

Figure 4.7b shows the concentration profile after 36 s. The experimental and numerical results exhibit the same physical phenomena. The maximum area of concentration is located around the top corner of the grid part. Behind the baffles, the mixing has not yet

proceeded although the mixed region now extends to the wall. The reaction has already taken place in the bulk and the inside of the vessel can clearly be seen.

Figure 4.7c confirms the appearance of two segregation zones at the bottom of the tank. Although the segregations behind the baffles disappear with time, the presence of unmixed regions persists close to the free surface in the baffled configurations.

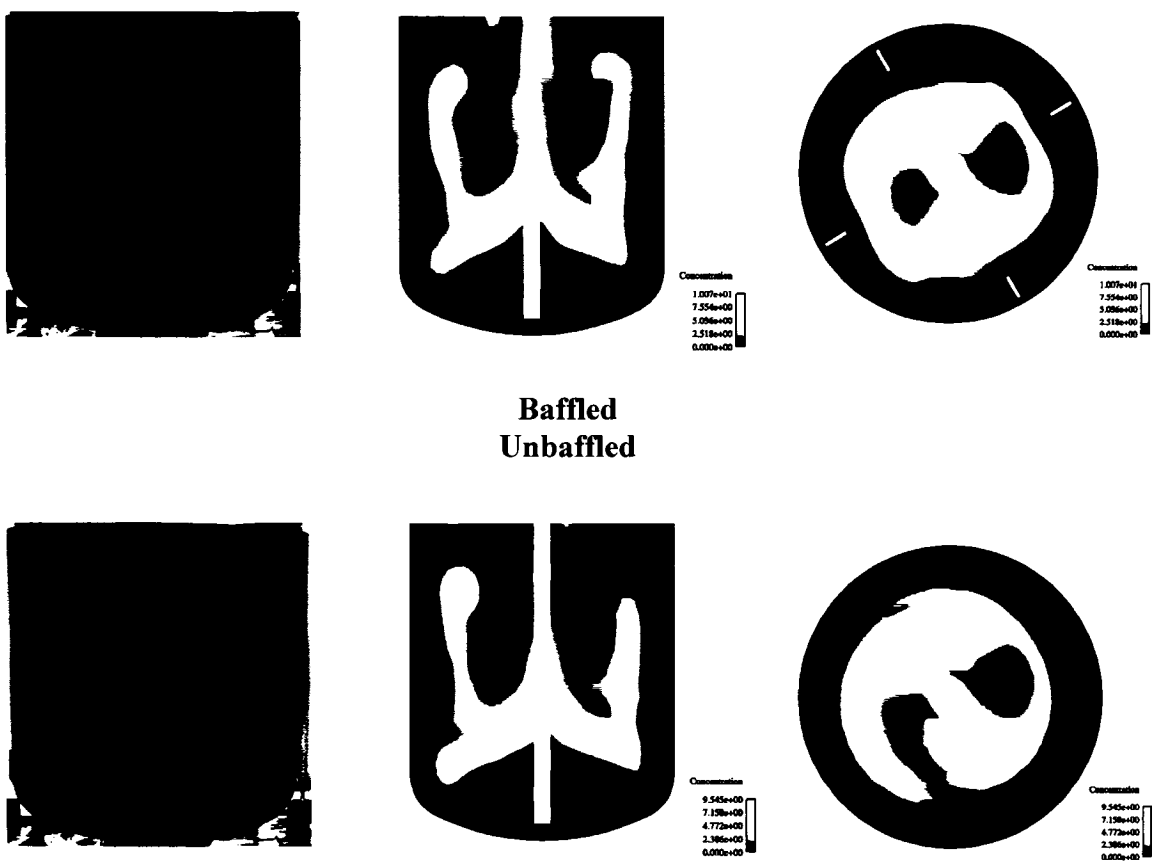

Figure 4.7 (a) Experimental and numerical results of discoloration technique after 9 s (Re=34).

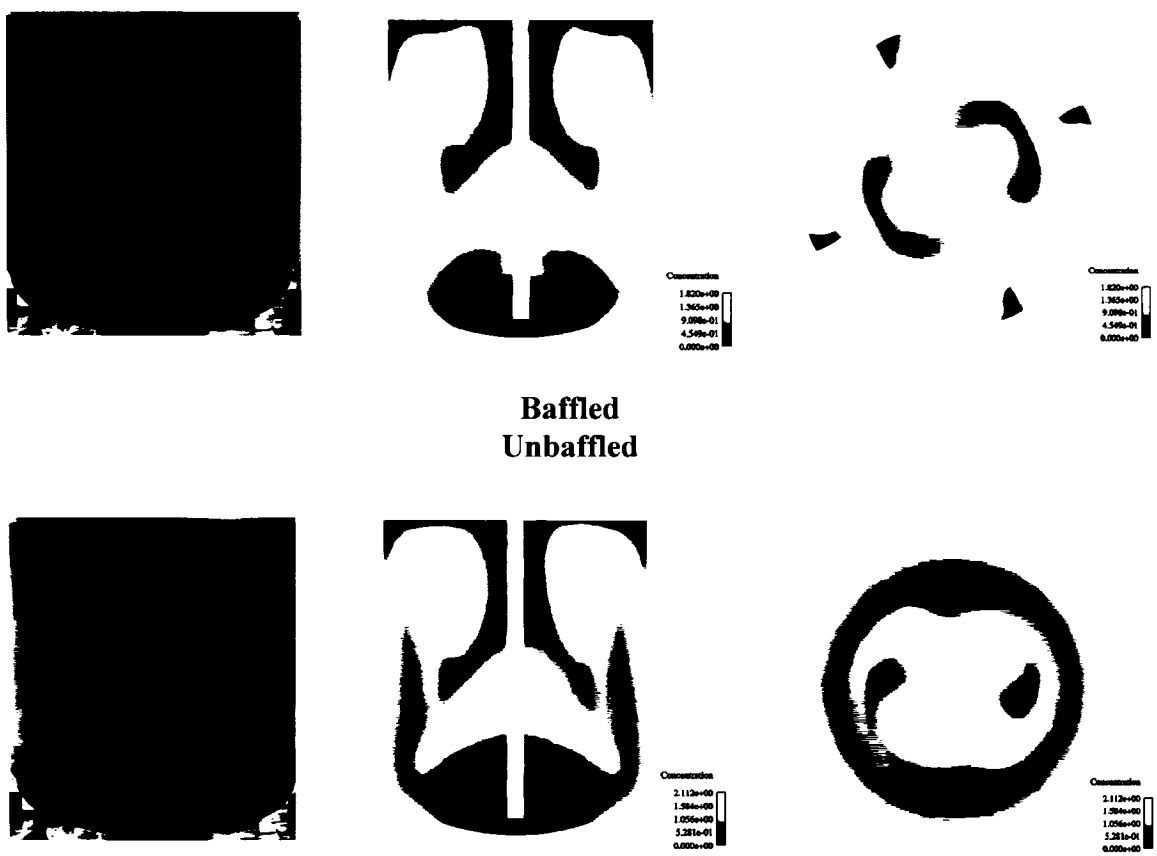

Figure 4.7 (b) Experimental and numerical results of discoloration technique after 36 s (Re=34).

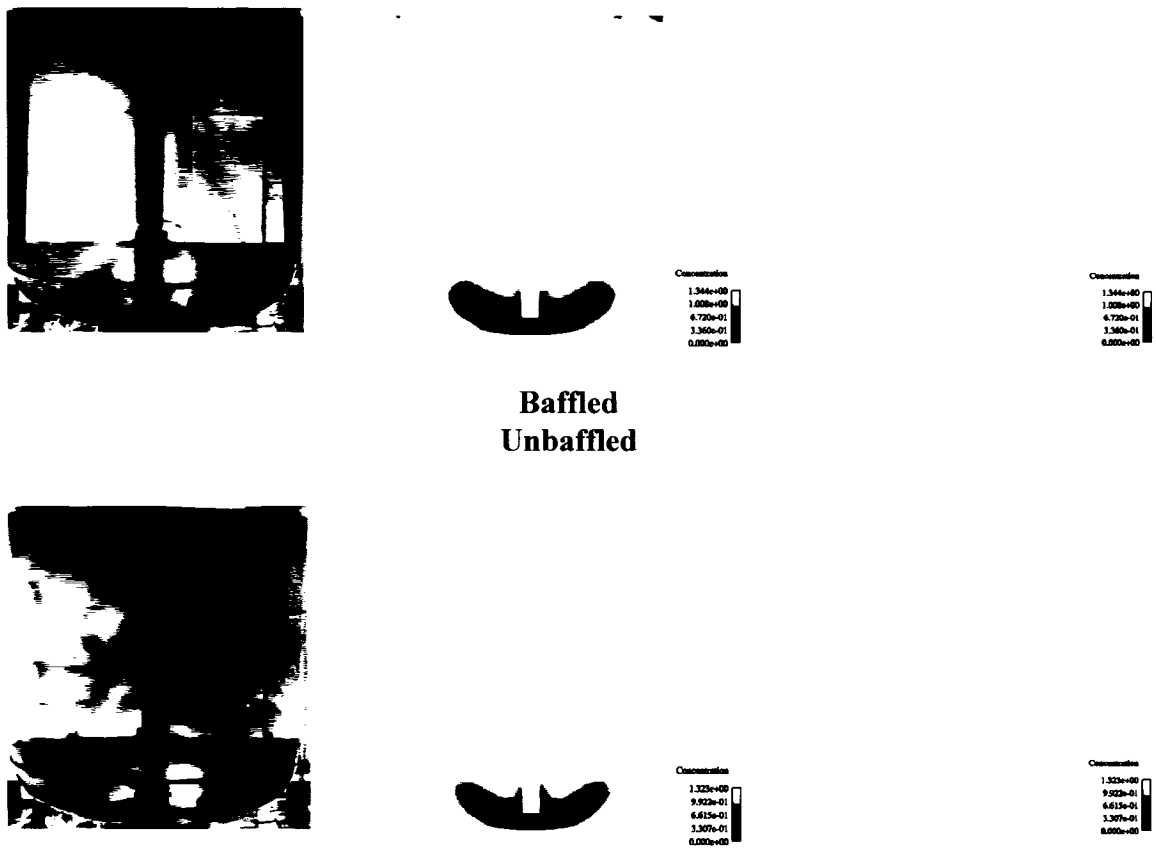

Figure 4.7 (c) Experimental and numerical results of discoloration technique after 48 s (Re=34).

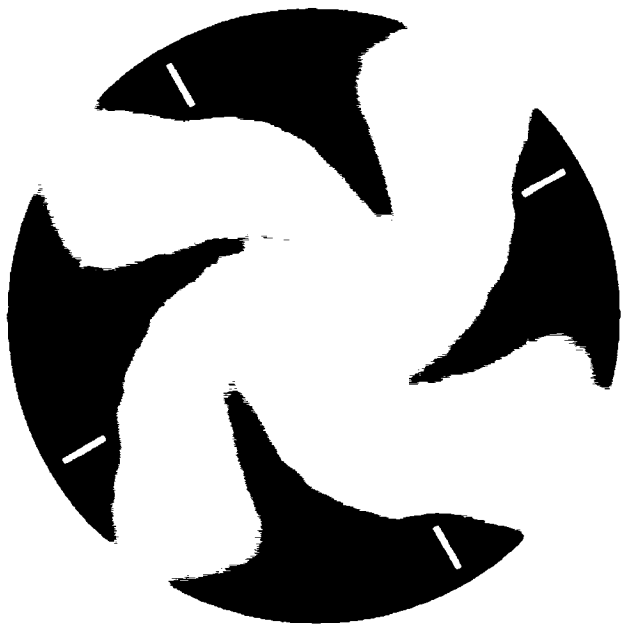

Figure 4.8 Horizontal cross section of concentration profile at free surface after 48 s (Re=34).

Figure 4.8 shows the horizontal cross section at the free surface of the baffled configuration system after 48 s. The segregated zones located in the vicinity of the baffles will disappear gradually; they can be easily eliminated by reducing the top clearance of the mixer.

Although the mixing mechanism at *Re*=34 seems to be similar for both configurations, the baffles become more effective in the homogenization process when the Reynolds number is increased.

4.4.6 Macro-mixing kinetics

As described in section 2, an image analysis method was utilized to quantify the macro-mixing kinetics in the system. Figure 4.9 shows a comparison of the mixing kinetics curve for baffled and unbaffled configuration at *Re*=70. Typically, a mixing kinetics curve can be divided into three regions. The first region, where the slope of the line is zero, corresponds to the period where no change in color can be observed by the discoloration technique. The second region represents the time at which the mixing starts to be effective, generating a noticeable color change, i.e. macro mixing phenomena. The third region, where the curve becomes asymptotic, is the time where the mixing is governed by micro mixing. We refer to the beginning of this region as the (macro) mixing time.

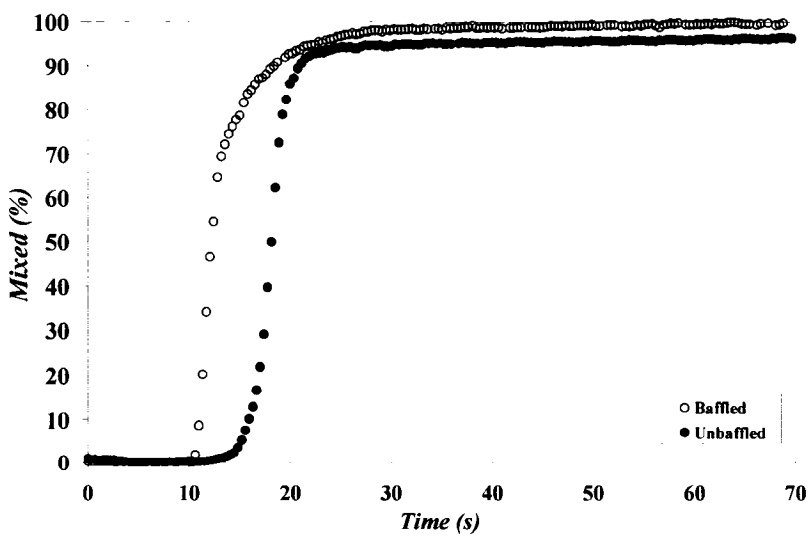

Figure 4.9 Comparison of kinetics curve for unbaffled and baffled configurations (Re=70).

In order to analyze the mixing kinetics curves of the mixer, a four parameter model has been used (Cabaret et al., 2006):

$$M = M_{\infty}\left(1-\left(1+(\frac{t}{\tau})^{a}\right)^{-n/a}\right) \tag{4.9}$$

where M is the percentage of mixed region, M_{∞} represents the vertical asymptotic value of M at third region, where the curve turns to a line with the slope of zero. The higher M_{∞}, the larger is the mixed region. The parameter τ represents the time at which the mixing starts to be effective and generates a noticeable color change. The exponent a scales the sharpness in the transition from first region towards second region in the mixing kinetics curve. The higher the value of a, the sharper is the transition. The exponent n represents the slope of the curve during the fast color change. This slope is a clear indication of the impeller capacity to generate efficient mixing.

Table 4.2 Comparison of kinetics curves model parameters for both configurations (Re=70).

	M_{∞} (%)	τ (s)	a	n
Unbaffled	95.47	18.19	19.14	21.99
Baffled	98.97	10.69	122.12	4.93

The resulting model parameters for both configurations are presented in Table 2. Generally, the baffles accelerate the discoloration process (Figure 4.9). As appears in τ, the baffled configuration starts its color changing 7 s sooner than the unbaffled configuration. In addition, the values of a indicate the sharp transition created by baffled configuration. Focusing on the second region (noticeable color change), both configurations have almost the same slope during the linear part, however, at the end of the color change they act differently. The unbaffled configuration exhibits a rapid and sharp transition to the third region; in contrast, due in part to presence of unmixed regions close to the free surface (Figure 4.8), the baffled configuration shows a curvature at the end of second region that highly affects the value of n. Finally, the baffled configuration achieves a full homogeneity (M_∞= 99 %) while the unbaffled configuration does not, due to the two bottom segregation zones (Figure 4.7c).

Figure 4.10 presents the experimental and numerical dimensionless mixing times for the two configurations. It appears that the dimensionless mixing time of the unbaffled configuration is 1.4 times larger than the one of baffled configuration. A good agreement is found between the experimental and numerical dimensionless mixing times with an average discrepancy of less that 12 % and 14 % for unbaffled and baffled configurations respectively. The numerical results presented in Figure 4.10 will be discussed further in the next section.

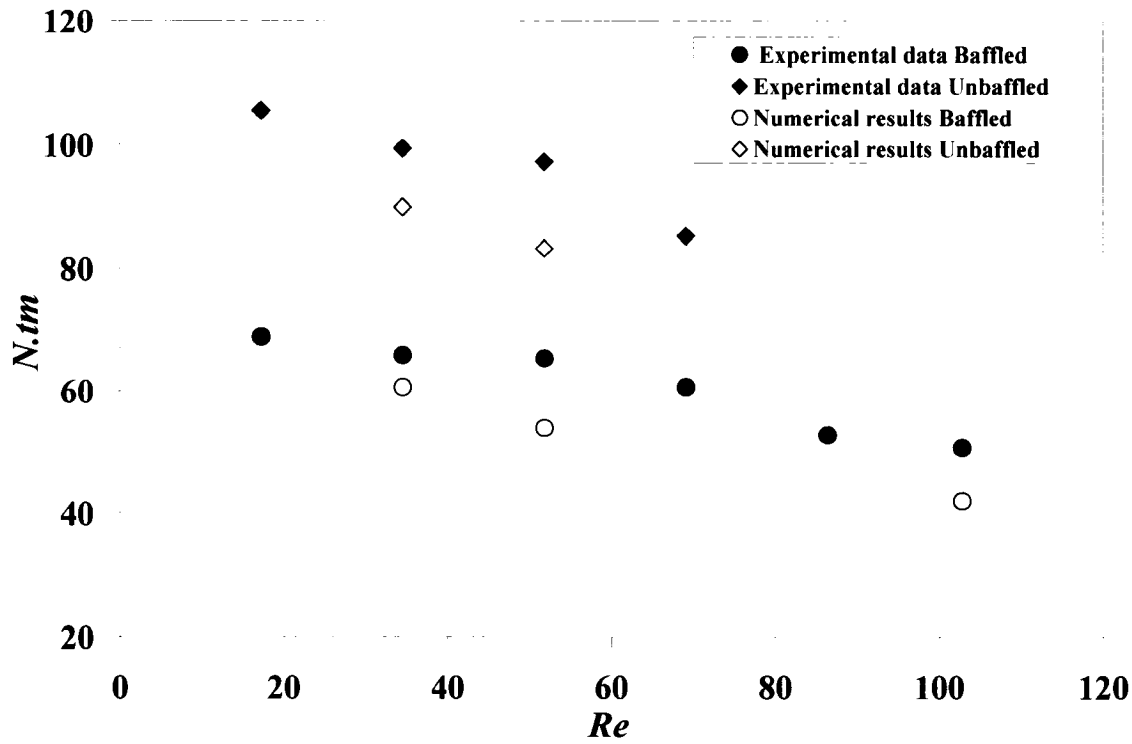

Figure 4.10 Experimental and numerical dimensionless mixing times for both configurations.

4.4.7 Intensity of segregation

In order to further analyze the results obtained from the simulation and determine precisely the numerical mixing time, the intensity of segregation concept was also utilized, which consists of studying the dispersion of concentration in the tank. The intensity of segregation is defined (Danckwerts,1952) as

$$I_{seg} = \frac{1}{\overline{C}(1-\overline{C})} \frac{1}{V_{Total}} \sum_{i=1}^{K} (C_i - \overline{C})^2 V_i \tag{4.10}$$

where K is the number of elements, and $\overline{C}$ is the mean concentration value, C_i is concentration value in each finite element i, V_i is the volume of this element and V_{Total} denote similar quantities for the whole domain. The value of I_{seg} is between 0 (optimal dispersion) and 1 (complete segregation).

The values of C_i, the concentration, were obtained from two different methods. The first method consists of using the nodal value of concentration from the mass transfer solution. The second method similar to our past work (e.g. De La Villeon et al. 1998; Iranshahi et al. 2006), based on computation of the dispersion of a cluster of tracers in the tank. The concentration of tracers C_i in each finite element i can be calculated at each time step as

$$C_i = \frac{N_i V_{Total}}{N_{Total} V_i} \tag{4.11}$$

where N_i denotes the number of tracers in element i, N_{Total}, is the same for the whole domain.

The results obtained are presented in Figure 4.11a-d. A cluster of 5000 tracers was launched and their position was computed using the element-by-element predictor-

corrector shooting scheme (Heniche & Tanguy, 2006). Figure 4.11a-b show the intensity of segregation for baffled and unbaffled configurations based on mass transfer simulation. It can be noticed that at the initial time, the intensity of segregation (t=0) is less than 1. The reason for this phenomenon is that the volume occupied by the initial injection is larger than the volume of one element of the mesh. At the beginning of the mixing when concentration distribution is highly affected by bulk mass transfer, the intensity of segregation curve shows an oscillating behavior. The intensity of segregation then reduces hyperbolically versus time, corresponding to the period where both bulk and diffusive mass transfer mechanisms evolve during the agitation. Finally, the curve becomes asymptotic, where the mixing is governed by diffusion.

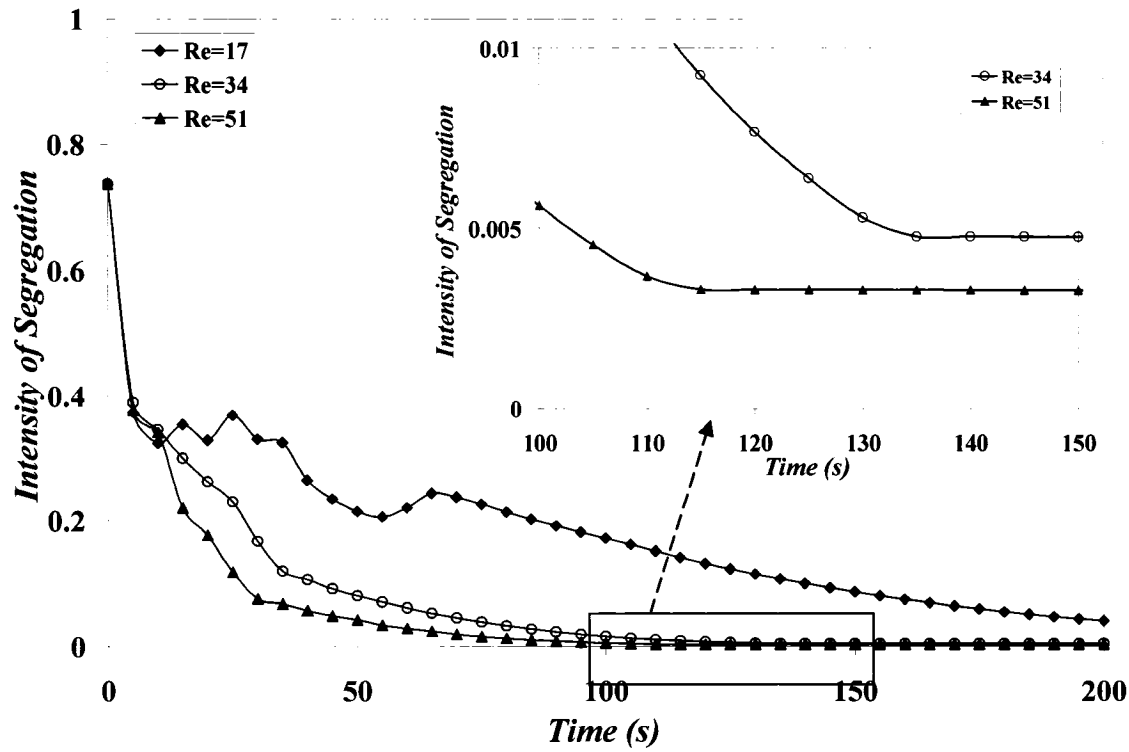

Figure 4.11 (a) Numerical intensity of segregation vs. time based on mass transfer simulation for unbaffled configuration.

The time at which the curves level off (the beginning of the linear region) corresponds to the mixing time. As expected, increasing the Reynolds number decreases the mixing time. For both unbaffled and baffled cases, the period of observation is not long enough to stabilize the intensity of segregation at *Re*=17. Moreover, the values of the intensity of segregation after reaching the corresponding mixing times are almost identical at different Reynolds numbers for each configuration.

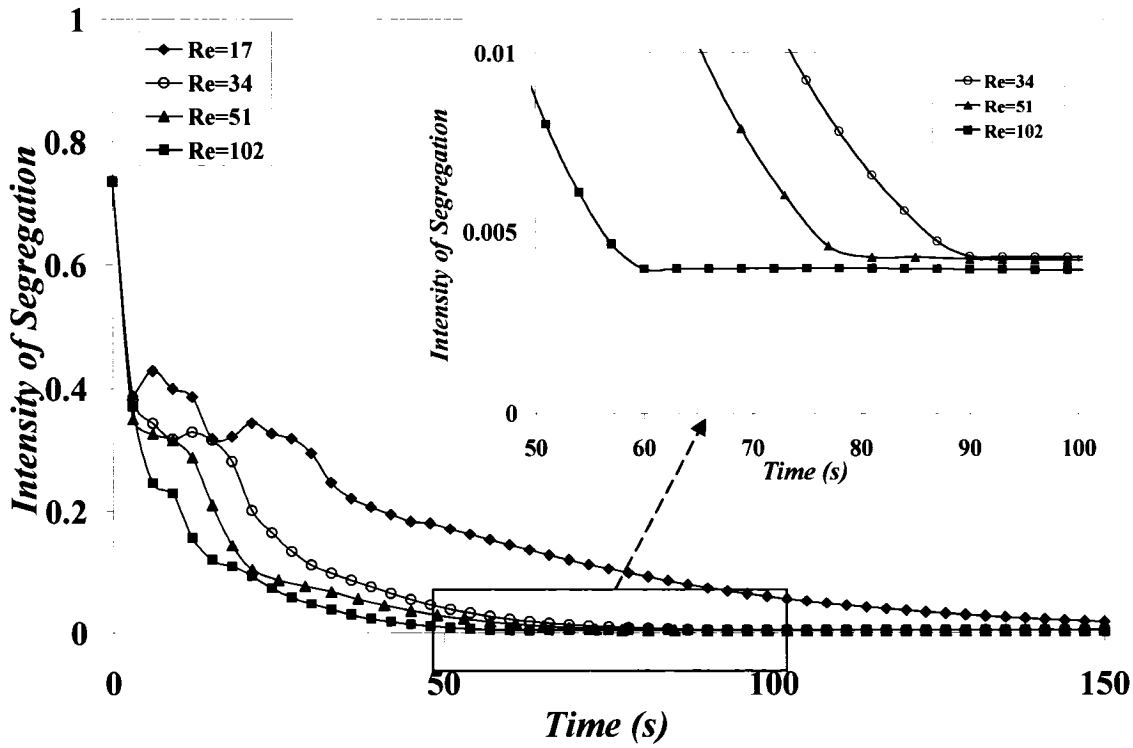

Figure 4.11 (b) Numerical intensity of segregation vs. time based on mass transfer simulation for baffled configuration.

Figure 4.11c shows the values of the intensity of segregation for both configurations at *Re*=51. It highlights the experimental observation that baffles cause more "chaotic" mixing and decrease the mixing time, since the baffles curve has always the lower value of the intensity of segregation, and it reaches to its final value sooner than the unbaffled curve.

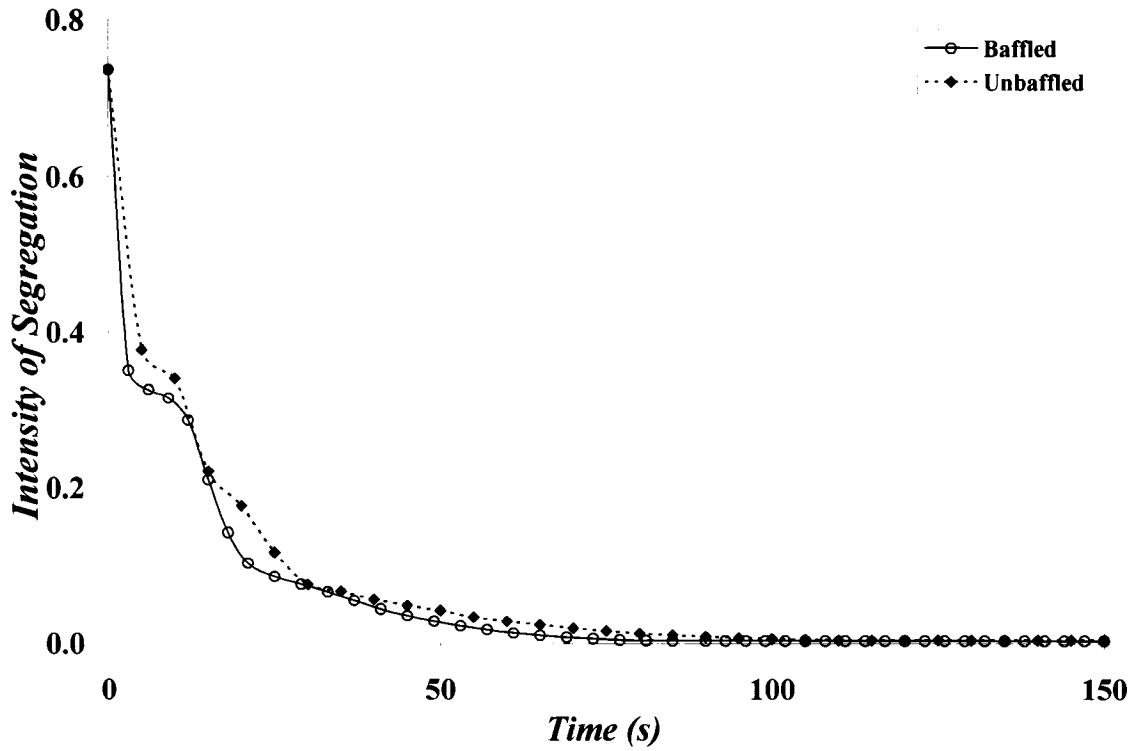

Figure 4.11 (c) Comparison of numerical intensity of segregation based on mass transfer simulation for baffled and unbaffled configuration (Re=51).

In contrast with our past work (e.g. Iranshahi et al., 2006), the time varying intensity of segregation obtained from trajectory calculation exhibits permanent oscillations that make it difficult to establish the mixing time. Figure 4.11d shows a comparison of the numerical intensity of segregation from mass transfer solution and trajectory calculation for baffled configuration at *Re*=51. The cluster of tracers in the trajectory calculations was injected at the same point as for the mass transfer problem. The mass transfer

simulation results show a much smoother behavior closer to the real physics than the classical massless particle trajectory analysis.

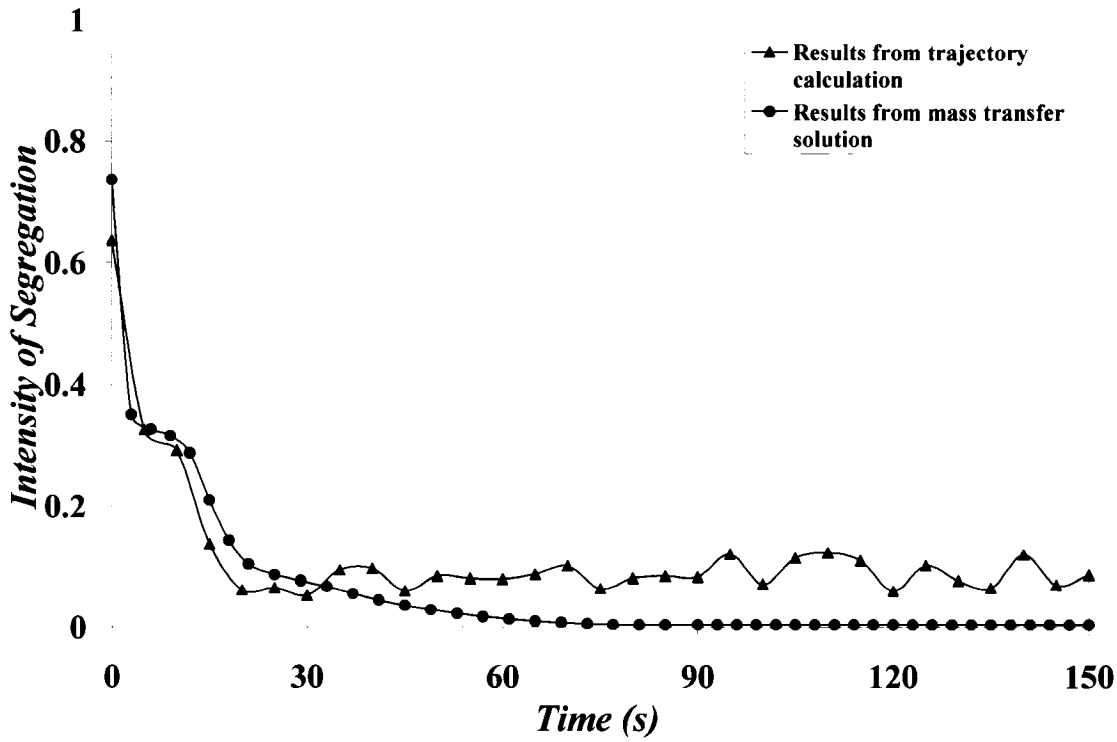

Figure 4.11 (d) Comparison of numerical intensity of segregation from mass transfer solution and trajectory calculation for baffled configuration (Re=51).

We do not show the intensity of segregation results for the injection point at the paddle (bottom) structure. Indeed, it was found that the intensity of segregation in this case neither stabilizes nor decreases during the period of study. This phenomenon was

expected due to the flow segregation at the bottom. Intensity of segregation calculation illustrates again the existence of the two independent mixing structures.

4.4.8. Mixing efficiency

In the laminar regime, the mixing performance is mainly related to the stretching rate of fluid lines or fluid interfaces. Using this concept, Ottino (1989) developed a quantitative criterion, the local efficiency of mixing:

$$e_\lambda = \frac{\mathrm{D}\ln\lambda/\mathrm{D}t}{\left(\dot{\underline{\underline{\gamma}}}:\dot{\underline{\underline{\gamma}}}\right)^{1/2}}, \tag{4.12}$$

where

$$\lambda = \lim_{\|dX\|\to 0}\frac{\|dx\|}{\|dX\|} \tag{4.13}$$

is the so-called stretching and $\mathrm{D}./\mathrm{D}t$ is the material derivative. In this expression, dX is an initial segment and dx is the same segment but stretched during a sufficiently long period of time t. It can be proven that e_λ is frame independent.

For purely viscous fluids, $\left(\dot{\underline{\underline{\gamma}}}:\dot{\underline{\underline{\gamma}}}\right)^{1/2}$ is related to the viscous dissipation. In the case of Newtonian fluids, the mixing efficiency can then be interpreted as the fraction of the energy dissipated locally for stretching fluid elements. A negative value indicates that

the energy dissipated is used to shorten the length of a material line, while a positive value indicates that the energy dissipated is used to stretch a material line. An effective mixer requires high values of stretching λ over time. Alternatively, mixer efficiency can be quantified by computing the corresponding time-averaged mixing efficiency:

$$< e_\lambda >= \frac{1}{t}\int_0^t e_\lambda \, dt \quad . \tag{4.14}$$

The time-averaged mixing efficiency varies with time as t^{-1} for flows with no reorientation and some flows with periodic reorientation, whereas flows with strong reorientation generally exhibit a curve that oscillates around a constant value of this efficiency (Ottino 1989).

In this work, time-average mixing efficiencies were computed for both configurations by averaging out the values obtained using 6,138 segments of 1 μm length corresponding to 279 initial positions and 22 directions.

Figure 4.12a shows the time-averaged mixing efficiency for a mid-height (H=0.35 m) injection point at *Re*=51. The mixing efficiency curves provided in Figure 4.12a show that the both configurations fall into the category of mixer that exhibit periodic flow reorientation with a time-decaying time-averaged mixing efficiency (Ottino, 1989). Although the baffled configuration shows a better mixing efficiency than the unbaffled

configuration at the beginning, the two curves level off to similar values after approximately 2 minutes of agitation corresponding to 80 impeller rotation.

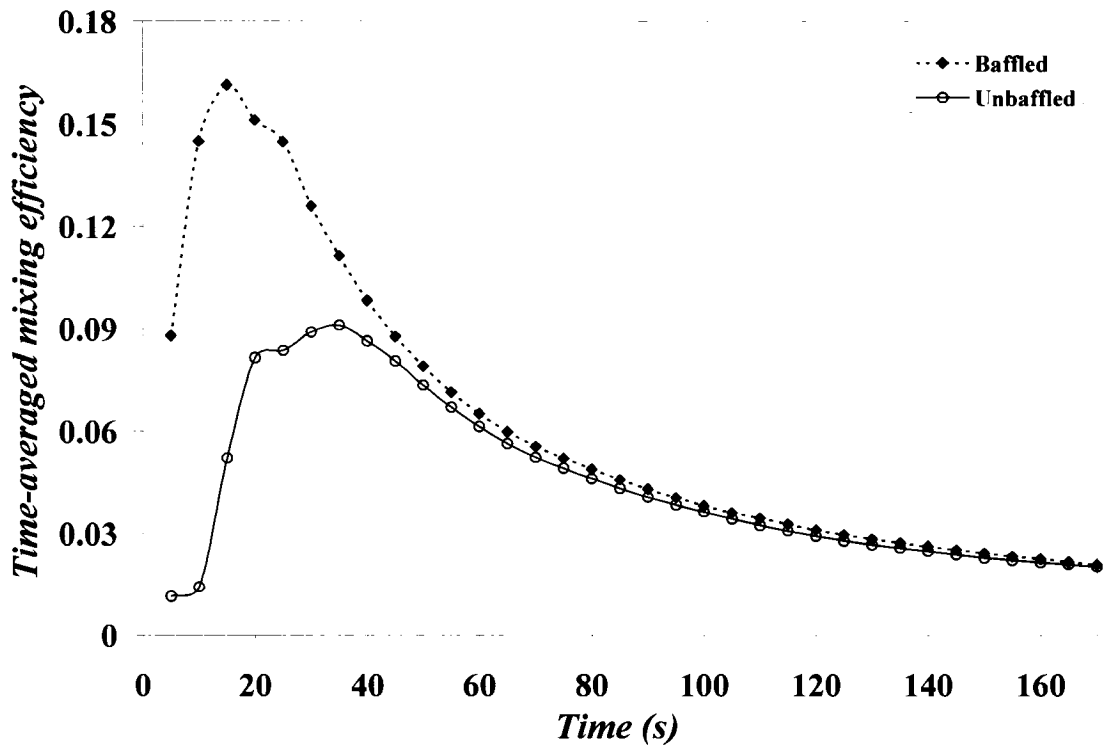

Figure 4.12 (a) Time-average mixing efficiency vs. time (mid-height injection point, Re=51).

Figure 4.12b shows the time-averaged mixing efficiency for the bottom injection point (H=0.1 m) at *Re*=51. For this injection point both configurations have similar behavior as the mid-height injection. The results show that overall both paddle and grid structures

have the same local mixing efficiency, however, the weakness of mass transfer between these two structures at low Reynolds numbers is probably the main cause of the numerically and experimentally observed unmixed area at the paddle region.

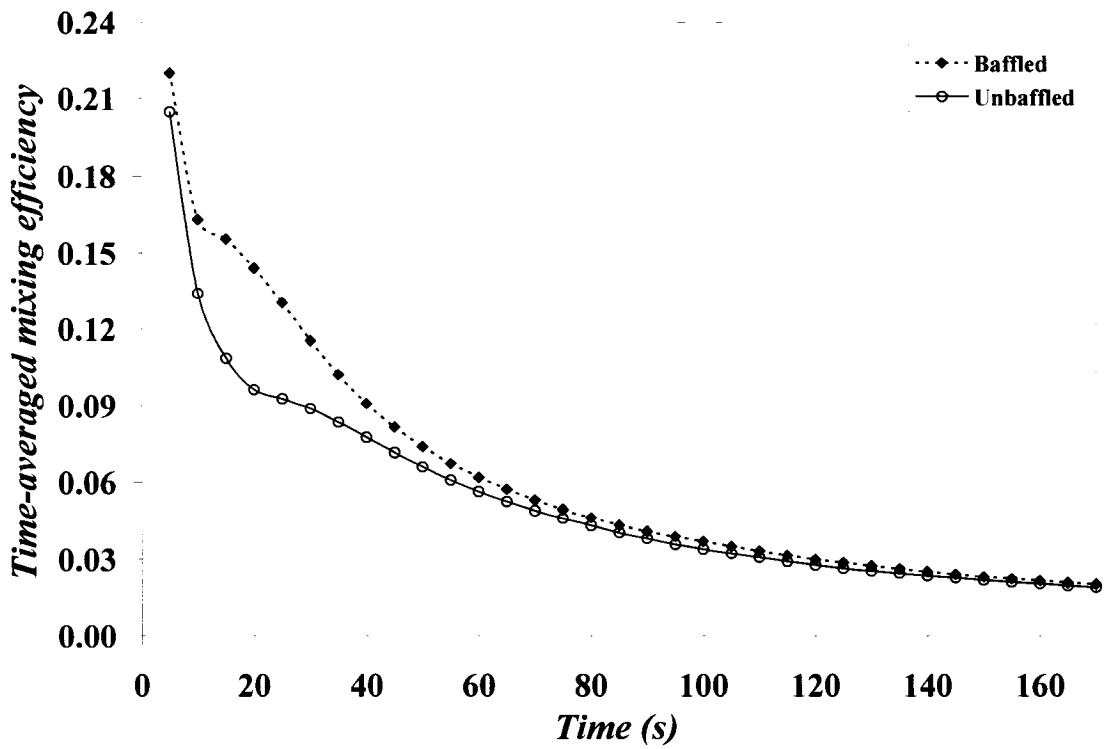

Figure 4.12 (b) Time-average mixing efficiency vs. time (bottom injection point, Re=51).

4.5 Conclusion

The objective of this paper was to investigate experimentally and numerically the flow and mixing in a vessel equipped with a Maxblend impeller in the laminar and transition regimes with Newtonian fluids. The Maxblend configuration included both an unbaffled version and a fully baffled installation with 4 baffles. The experimental and numerical investigations were carried for Reynolds numbers up to 100. In the experimental study, the power consumption and the mixing time (discoloration technique coupled by advance image analysis method) were investigated. The numerical results for the power consumption and mixing time were validated with experimental data. Computational techniques were applied to study the evolution of mixing patterns and predict the shear rate distribution, pumping capacity, concentration profile, intensity of segregation, mixing time and mixing efficiency and the results of both baffled and unbaffled configurations were compared to each other. It was shown that despite the complex flow field created by the impeller, homogeneous mixing is not achieved at low Reynolds numbers and two segregation zones at the bottom of the tank are created. At higher Reynolds numbers, a fast and homogeneous mixing can be achieved. However, a strong vortex is created with the unbaffled configuration, which constrains the practical operation. In conclusion, the Maxblend reveals good performance when used with baffles in the transition regime and upper laminar regime.

4.6 Acknowledgements

The financial assistance of the Natural Science and Engineering Research Council of Canada (NSERC) is gratefully acknowledged.

CHAPTER 5

ADDITIONAL RESULTS

5.1 Introduction

This chapter consists of the addition experimental and numerical data that for brevity are not included in the article. The chapter follows the same structure as article and mentions the additional useful information.

5.2 Experimental results

5.2.1 Vortex effect on unbaffled operation

A strong vortex appears when unbaffled operation exceeds *Re*=51. By increasing the Reynolds up to 86, undesired air intake phenomenon appears (figure 5.1). Due to this

operational constrain, it was not possible to carry out the mixing time experiment for Reynolds higher than 70 for unbaffled configuration. On the other hand, the bottom segregation zones were observed for this configuration where Reynolds is less than 70. Therefore, unbaffled configuration always has segregation at the bottom unless operating under the air intake condition. However, the baffled configuration achieves a full homogenization status above *Re*=51. In conclusion, it is highly recommended to operate the Maxblend with baffles at Reynolds higher than 50 so that to ensure a full and fast blending.

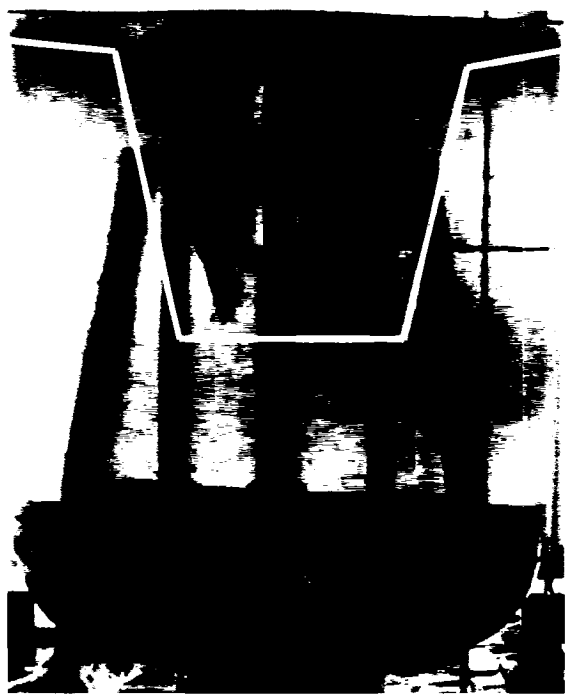

Figure 5.1 Air intake phenomena for unbaffled configuration (Re=102).

5.2.2 Effect of baffles at low Reynolds numbers

Although, traditionally baffles are considered to have no effect on deep laminar mixing performances, the results obtained with Maxblend is different. Figure 5.2 compares mixing performances of both configurations during the discoloration experiment at Re=17. The circular segregation zone around the higher edge of the Maxblend impeller in unbaffled configuration clearly proves the effect of baffles even in deep laminar regime. This phenomenon may be caused by the unique straight shape of the impeller.

Figure 5.2 Effect of Baffles at low Reynolds number (Re=17, t= 189 s).

5.2.3 Mixing mechanism of baffled configuration at high Reynolds numbers

Figure 5.3 shows a series of experimental photos of the discoloration process for the baffled configurations at *Re*=51. These figures reveal how the acidic fluid invades the

tank and shows the location of the two little segregated zones at the bottom and more specifically explains how these segregation zones will disappear.

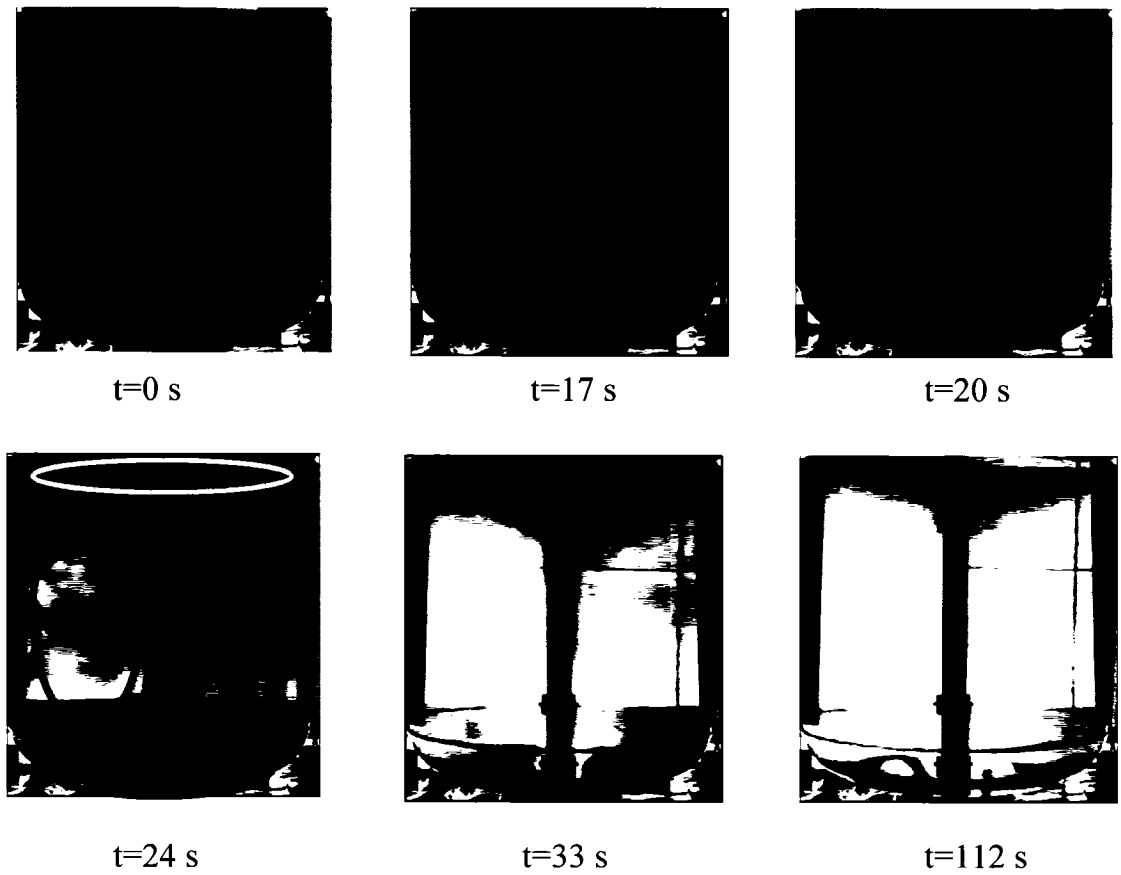

Figure 5.3 Experimental results of discoloration technique for baffled configuration (Re=51).

The first photo shows Maxblend at t=0 while the fluid is at rest. After 17 second the color changing process starts and till the 27 s the majority of discoloration occurs. Three

different mixing zones can be clearly seen at t= 24 s, one close to the free surface, the other at the grid part and the last one at the bottom. The figure at t=33 s confirms the appearance of two segregation zones at the bottom of the tank. Finally, the last figure reveals how the impeller starts to mix the segregation zones by make them hollow. The segregation zones then will disappear after limited rotation of the impeller.

5.3 Numerical results

5.3.1 Flow and pumping patterns

Figure 5.4 compares the axial velocity field in elevated surface for the unbaffled configuration at different Reynolds numbers. Although the paddle at the vessel bottom produces a weak axial flow, the grid part generates an efficient axial pumping, with an upward motion at the vessel wall and a downward flow along the shaft. Figure 5.5 compares the contour of the constant axial component surface of the 3D velocity field for unbaffled configuration at different Reynolds numbers. Both Figures 5.4-5.5 illustrate that as the Reynolds increases, the impeller axial pumping increases.

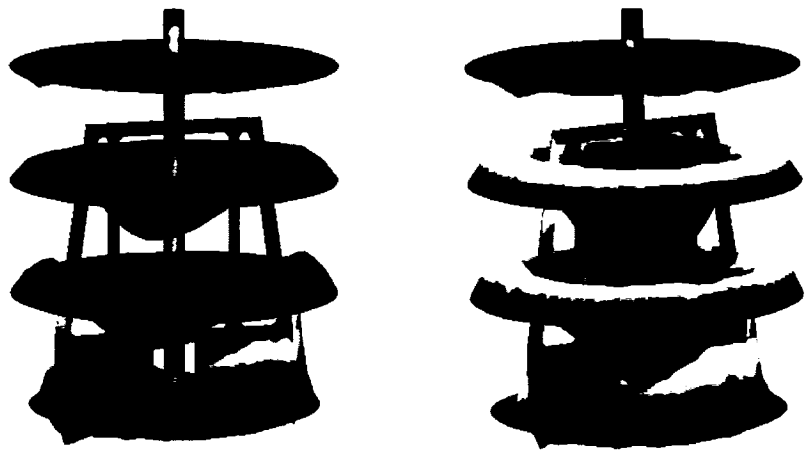

Re=40 Re=80

Figure 5.4 Comparison of contour of the axial component of the 3D velocity field for unbaffled configuration at different Reynolds numbers.

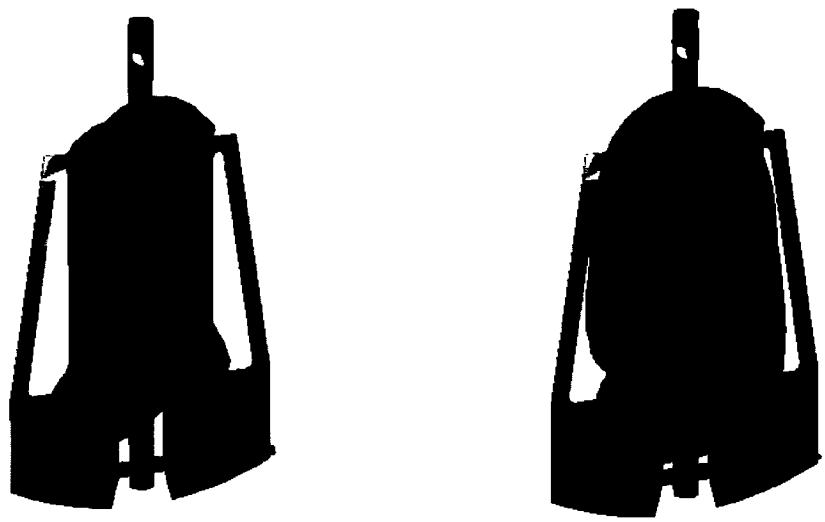

Re=40 Re=80

Figure 5.5 Comparison of contour of the constant axial component surface of the 3D velocity field for unbaffled configuration at different Reynolds numbers.

5.3.2 Shear rate distribution and viscous dissipation

Figure 5.6 shows the contribution of the different components of the shear rate tensor for unbaffled configuration at Re=80. Although both $r\theta$ and $\theta\theta$ components of shear rate have high values, due to the direction of the rotation, impeller creates almost no shear at $z\theta$ direction. Figure 5.7 compares contour of $r\theta$ component of 3D deformation for both configurations at Re=51.

The impeller surface is the zone where the shear rate is the largest of the domain with the maximum at the two bottom corners of the paddle. In addition, baffled configuration illustrates higher and more complicated shear rate distribution compared to unbaffled configuration. Figure 5.8 shows the contour of maximum area of viscous dissipation for unbaffled configuration (Re=80). It appears that the only area with a significant viscous dissipation is where the maximum shear rate occurs, namely the corner of the paddle part. In the other areas of the domain, viscous dissipation is negligible.

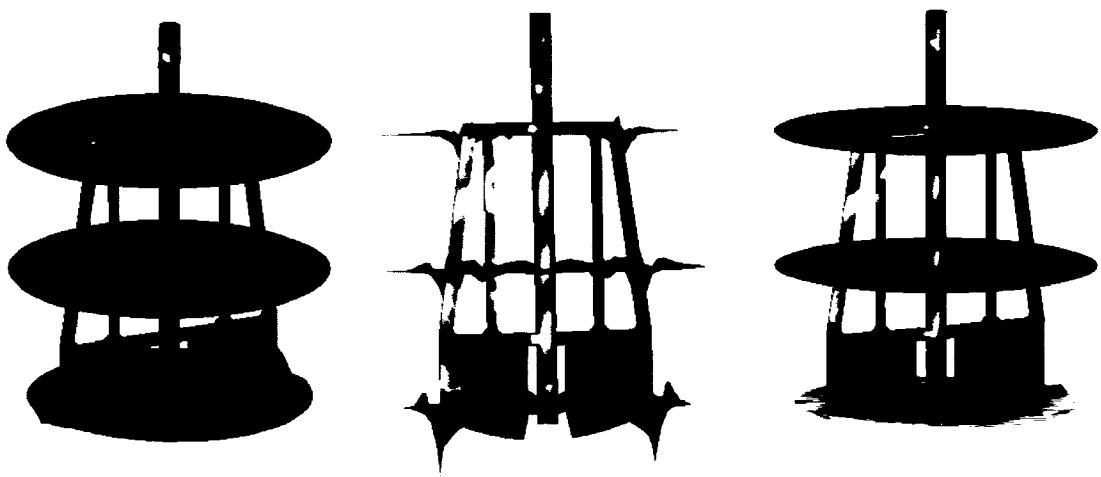

$r\theta$ $\theta\theta$ $z\theta$

Figure 5.6 Contour of different component of 3D shear rate (Re=80).

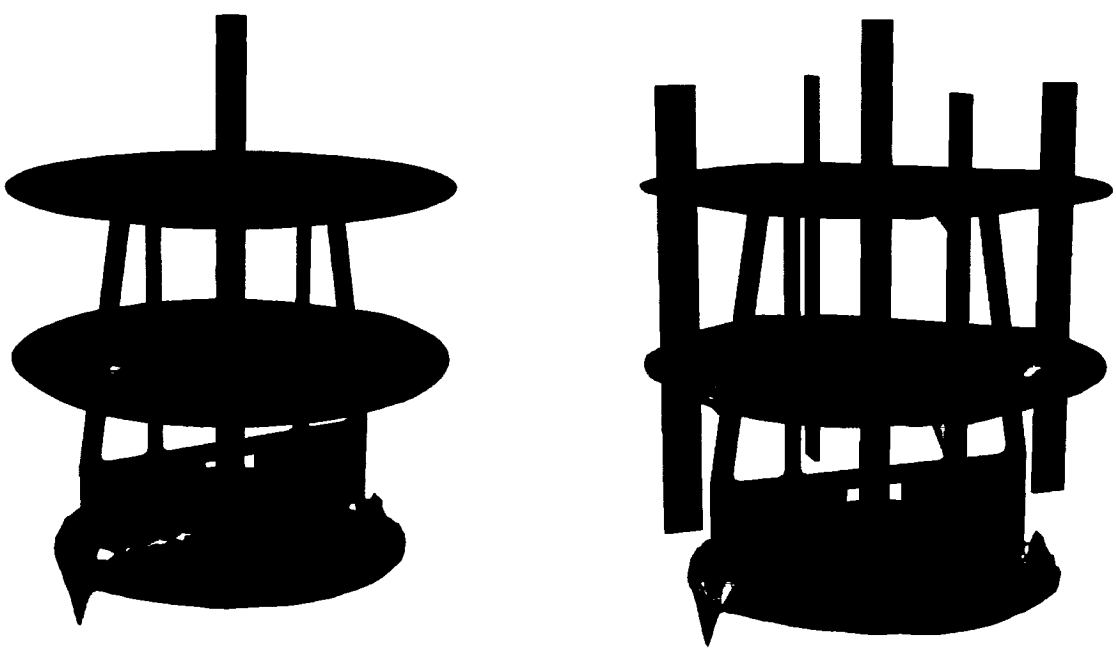

Figure 5.7 Contour of $r\theta$ component of 3D deformation (Re=51).

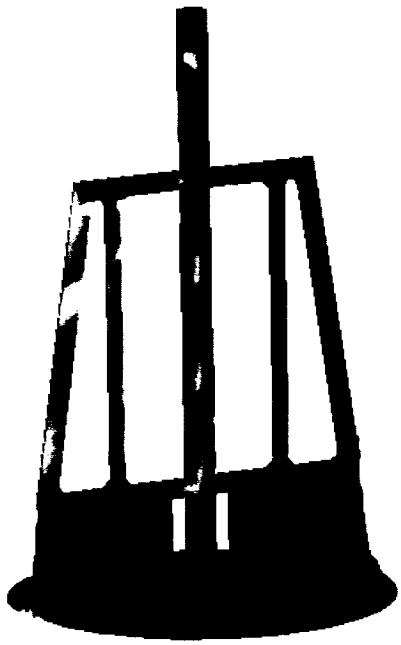

Figure 5.8 Contour of maximum area of viscous dissipation for unbaffled configuration (Re=80).

5.3.3 Trajectory calculation

The results presented in figures 5.9-5.10 shows a cluster of 10 tracers, injected at two different positions, one at paddle part and the other at grid part. Once again, the pervious experimental and numerical observation of existence of segregation at the bottom is confirmed. Figure 5.9 shows the trajectory calculation results for paddle injection point where the particles stay at the bottom and never go to the upper part of the tank. In parallel, figure 5.10 illustrates the results obtained from the grid part injection point where particles never move to the bottom part of the tank.

Figure 5.9 Trajectory calculation results for paddle injection point (Re=60).

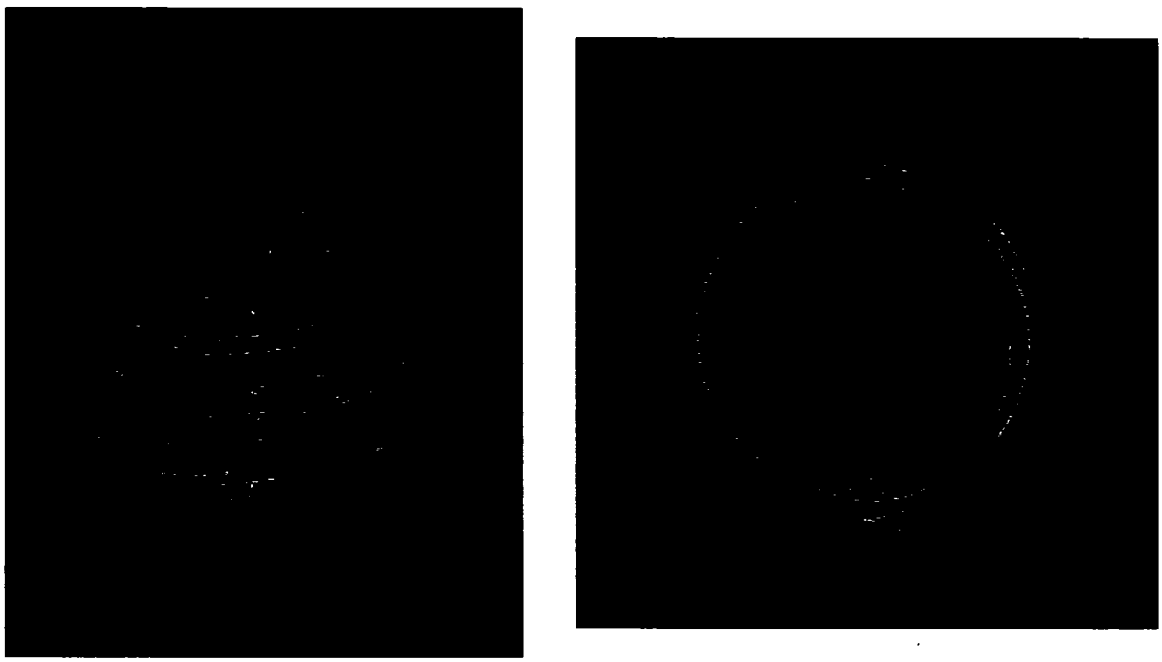

Figure 5.10 Trajectory calculation results for grid injection point (Re=60).

CHAPTER 6

GENERAL DISCUSSION

In this work, we wanted to shed some light on the flow and mixing in a vessel equipped with a Maxblend impeller in the laminar and transition regimes. The flow field and the mixing structures were studied both numerically and experimentally. The power consumption and the mixing kinetics were evaluated both by means of experiment and computation and the numeric results were validated by comparisons with experimental data. Computational techniques were applied to the evolution of mixing patterns and predict mixing capability of the impeller. It was shown that despite the complex flow field created by the impeller, homogeneous mixing is not achieved for highly viscous materials. Indeed the impeller has not been designed for this range of Reynolds number. It was shown that a separation plane exists in the tank at end of the grid from the top at low rotational speed. Convective mixing is very slow at low agitation rate across this plane.

CHAPTER 7

CONCLUSION AND RECOMMENDATIONS

The objective of this work was to investigate experimentally and numerically the flow and mixing in a vessel equipped with a Maxblend impeller in the laminar and transition regimes. The Maxblend performance for Newtonian fluids were studied in two configurations namely, unbaffled configuration and baffled configuration. The experimental and numerical investigations were carried for Reynolds numbers up to 100. In the experimental study, the power consumption and the mixing kinetics (discoloration technique coupled by advance image analysis method) were investigated. The numerical results for the power consumption and mixing time were validated with experimental data. Computational techniques were applied to study the evolution of mixing patterns and predict the shear rate distribution, pumping capacity, concentration profile, intensity of segregation, mixing time and mixing efficiency and the results of both baffled and unbaffled configurations were compared to each other. It was shown that despite the complex flow field created by the impeller, homogeneous mixing is not achieved at low

Reynolds numbers and two segregation zones at the bottom of the tank are created. Indeed the impeller has not been designed for this range of Reynolds number. While baffled configuration, at high Reynolds numbers, achieves fast and homogeneous mixing, a strong vortex created by unbaffled configuration, constrains the operation at high Reynolds numbers.

In conclusion, it is highly recommended:

a) To avoid vortex and air intake phenomenon, unbaffled configuration operation not exceeds Re=51.
b) To achieve full homogenization status the baffled configuration operates at Reynolds higher than 51.

Following the investigations described in this thesis, a number of projects could be recommended, involving the Maxblend mixer:

- Further investigation of the Maxblend performance while changing the top and bottom clearances;
- It would be interesting to combine the Maxblend with open impellers in different configurations (dual shaft configuration, dual impellers with one shaft configuration);
- Investigation of the Maxblend performance for multiphase applications;

REFERENCES

Alvarez-Hernandez, M. M., Shinbrot, T., Zalc, J., and Muzzio, F. J. (2002). Practical chaotic mixing. Chemical Engineering Science, 57, 3749–3753.

Bakker, A., and Gates, L.E. (1995). Viscous mixing. Chemical Engineering Progress. 91, 25-34.

Bakker, A., Haidari, A.H., and Oshinowo, L.M. (2001). Realize greater benefits from CFD. Chemical Engineering Progress, 97, 45-53.

Bartels, C., Breuer, M., Wechsler, K., and Durst, F. (2002). Computational fluid dynamics applications on parallel-vector computers: computations of stirred vessel flows. Computers & Fluids, 31, 69-97.

Bertrand, F., Gadbois, M., and Tanguy, P.A. (1992). Tetrahedral elements for fluid flow problems. International Journal of Numerical Methods in Engineering , 33, 1251-1267.

Bertrand, F., Tanguy, P.A., and Thibault, F. (1997). A three-dimensional fictitious domain method for incompressible fluid flow problems. International Journal of Numerical Methods in Fluids, 25, 719-736.

Bertrand, F., and Tanguy, P.A. (2002). Krylov-Based Uzawa algorithms for the solution of the Stokes equations using discontinuous pressure tetrahedral finite elements. Journal of Computational Physics, 181, 617-638.

Brooks A.N., and Hughes, T.J.R. (1982). Stream upwind/Petrov-Galerkin formulation for convection dominated flows with particular emphasis on the incompressible Navier-Stokes equations. Computer Methods in Applied Mechanics and Engineering, 32, 199-259.

Cabaret, F., Fradette, L., and Tanguy, P.A. (2006). Characterization of macro-mixing kinetics using advanced image analysis. In: Proceedings of 12th European Conference on Mixing, Bologna-Italy, 391-398.

Cooley, J.W., and Tukey, J.W. (1965). An algorithm for the machine calculation of complex Fourier series. Mathematics of Computation, 19, 297–301.

Danckwerts, P. V. (1952). The definition and measurement of some characteristics of mixtures, Applied Scientific Research, A3, 279-296.

De La Villeon, J., Bertrand, F., Tanguy, P.A., Labrie, R., Bousquet, J., and Lebouvier, D. (1998). Numerical investigation of mixing efficiency of helical ribbons. AIChE Journal, 44, 972-977.

Dohi, N., Takahashi, T., Minekawa, K., and Kawase, Y. (2004). Power consumption and solid suspension performance of large-scale impellers in gas–liquid–solid three-phase stirred tank reactors. Chemical Engineering Journal, 97, 103–114.

Glowinski, R., Pan, T.W., and Periaux, J. (1994). A fictitious domain method for Dirichlet problem and applications. Computer Methods in Applied Mechanics Engineering, 111, 283–303.

Harnby, N., Edwards, M.F., and Nienow, A.W. (1992). Mixing in the process industries. Butterworth-Heinemann Ltd., Toronto.

Harris, C. K., Roekaerts, D., Rosendal, F. J. J., Buitendijk, F. G. J., Daskopoulos, Ph., Vreenegoor, A. J. N. and Wang, H. (1996). Computational fluid dynamics for chemical reactor engineering, Chemical Engineering Science , 51, 1569-1594.

Heniche, M., and Tanguy, P.A. (2006). A new element-by-element method for trajectory calculations with tetrahedral finite element meshes. International Journal of Numerical Methods in Engineering, 67(a), 1290-1317.

Hiruta, O., Yamamura, K., Takebe, H., Futamura, T., Iinuma, K., and Tanaka, H. (1997). Application of Maxblend fermentor for microbial process. Journal of Fermentation and Bioengineering, 83, 79–86.

Hughes, T.J.R., and Brooks, A.N. (1982). A theoretical framework for Petrov-Galerkin methods with discontinuous weighting functions: applications to the Streamline-Upwind procedure. Finite Elements in Fluids. Gallagher, R. H., Vol. 4, Wiley, London, 47–64.

Iranshahi, A., Heniche, M., Bertrand, F., and Tanguy, P.A. (2006). Numerical investigation of the mixing efficiency of the Ekato Paravisc impeller. Chemical Engineering Science, 61, 2609-2617.

Kouda, T., Yano, H., and Yoshinaga, F. (1997). Effect of agitator configuration on bacterial cellulose productivity in aerated and agitated culture Journal of Fermentation and Bioengineering, 83, 371-376.

Kuratsu, M., Yatomi, R., and Satoh, H. (1995). Design of versatile reactors. Chemical Equipment, 8, 86-92.

Lamberto, D.J, Muzzio, F.J., Swanson, P.D., and Tonkovich, A.L. (1996), Using time-dependent RPM to enhance mixing in stirred vessels. Chemical Engineering Science, 51, 733-741.

Mishima, M. (1992). New trend of mixing vessel. Chemical Engineering of Japan, 56,131-137.

Ottino, J.M. (1989). The kinematics of mixing: stretching: chaos and transport. Cambridge University Press, New York.

Saito, I., Honda, H., Kawabe, T., Mukumoto, F., Shimizu, M., and Kobayashi, T. (2000). Comparison of biotin production by recombinant *Sphingomonas* sp. under various agitation condition. Biochemical Engineering Journal, 5,129-136

Sumi, Y., and Kamiwano, M. (2001). Development and mixing characteristic of multistage impeller for agitating highly viscous fluid, Chemical Engineering of Japan, 34, 485-492.

Takahashi, T., Tagawa, A., Atsumi, N., Dohi, N., and Kawase, Y. (2006a). Liquid-phase mixing time in boiling stirred tank reactors with large cross-section impellers. Chemical Engineering and Processing, 45, 303–311.

Takahashi, K., Horiguchi, H., Mishima, M., and Yatomi, R. (2006b). Mixing characteristics in a vessel agitated by large paddle impeller Maxblend. In: Proceedings of 12th European Conference on Mixing, Bologna-Italy, C5.

Tanguy, P.A., Lacroix, R., Bertrand, F., Choplin, L., and Brito-De La Fuente, E. (1992). Finite element analysis of viscous mixing with a helical ribbon-screw impeller. AIChE Journal, 38, 939-944.

Tezduyar, T.E., Park, Y. J., and Deans, H. A. (1987). Finite element procedures for time-dependent convection-diffusion-reaction systems. International Journal of Numerical Methods in Fluids, 7, 1013-1033.

Thibault, F., and Tanguy, P. A. (2002). Power-draw analysis of a coaxial mixer with Newtonian and non-Newtonian 'uids in the laminar regime. Chemical Engineering Science ,57, 3861 – 3872.

Thomas, C.R. (1990). Problems of shear in biotechnology, Chemical engineering problems in biotechnology. M. A. Winkler, Elsevier Applied Sciences, UK, 23–94.

Wu, J., Graham, L.J., and Mehidi, N.N. (2006). Estimation of agitator flow shear rate. AIChE Journal., in press.

Yao, W., Mishima, M., and Takahashi, K. (2001). Numerical investigation on dispersive mixing characteristics of Maxblend and double helical ribbons. Chemical Engineering Journal, 84, 565-571.

Zienkiewicz, O.C., and Taylor, R.L. (2000). Convection dominated problems. The finite element method. 5th edition, vol. 2: McGraw-Hill, 438-505.

APPENDIX A

COMPUTATIONAL PROCEDURE FOR PUMPING CAPACITY

All the pumping computations in this study were done according to Heniche et al. (2005). This appendix consists of the mathematical procedure for pumping computation and explains how it is used for agitated tank applications.

The method involves generating horizontal *xy* cross-sections along the vertical direction to obtain the stream function ψ(x, y, z). The horizontal contribution of the flow rate, Q_{xy}, can then be calculated as

$$Q_{xy}(z) = (\psi_{max} - \psi_{min})\Delta z \qquad (A.1)$$

where Δz denotes the thickness of the volume element at vertical coordinate z, and ψ_{max} and ψ_{min} are the maximum and minimum values of the stream function on the

corresponding cross sectional planes. The total horizontal contribution of the flow rate along the tank height can be obtained by

$$Q_{xy}^{total} = \int_0^H (\psi_{max} - \psi_{min})dz \ , \qquad \text{(A.2)}$$

where H denotes the total height of the tank. It is also possible to calculate the r and θ components of the stream function in order to analyze the radial and tangential flows on cross sections.

Vertical flow or axial pumping can be characterized by Q_V on a given horizontal cross sectional plane of vertical coordinate z :

$$Q_V(z) = \iint_A |v_z^+| dA = \iint_A |v_z^-| dA, \quad dA = dxdy \qquad \text{(A.3)}$$

where A represents the cross sectional area of the horizontal plane, and v_z^+ and v_z^- are the upward and downward components of the velocity vector. Equation (A.3) implies the conservation of mass through the equality of upward and downward fluid flow rates. The average value of Q_V along the height of the tank is given by

$$Q_V^{ave} = \frac{1}{H} \int_0^H Q_V(z)dz \qquad \text{(A.4)}$$

The magnitude of Q_V^{ave} is a measure of the vertical secondary flows occurring during the rotation of the impeller.